# Fluvial bedrock gorges as markers for Late-Quaternary tectonic and climatic forcing in the Southwestern Alps

Thibaut Cardinal, Carole Petit, Yann Rolland, Laurence Audin, Stéphane Schwartz, Pierre Valla, Swann Zerathe, Régis Braucher

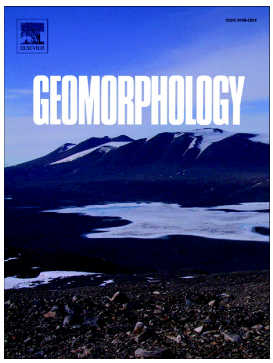


# Fluvial bedrock gorges as markers for Late-Quaternary tectonic and climatic forcing in the Southwestern Alps

Thibaut Cardinal, Carole Petit, Yann Rolland, Laurence Audin, Stéphane Schwartz, Pierre G. Valla, Swann Zerathe, Régis Braucher, ASTER team

PII: S0169-555X(22)00369-5

DOI: https://doi.org/10.1016/j.geomorph.2022.108476

Reference: GEOMOR 108476

To appear in: *Geomorphology*

Received date: 13 July 2022

Revised date: 28 September 2022

Accepted date: 28 September 2022

Please cite this article as: T. Cardinal, C. Petit, Y. Rolland, et al., Fluvial bedrock gorges as markers for Late-Quaternary tectonic and climatic forcing in the Southwestern Alps, *Geomorphology* (2022), https://doi.org/10.1016/j.geomorph.2022.108476

# Fluvial bedrock gorges as markers for Late-Quaternary tectonic and climatic forcing in the Southwestern Alps

**Thibaut Cardinal[1], Carole Petit[1], Yann Rolland[2-3], Laurence Audin[2], Stéphane Schwartz[2], Pierre G. Valla[2], Swann Zerathe[2], Régis Braucher[4], and ASTER team[4,*]**

*[1] Université Côte d'Azur, CNRS, Observatoire de la Côte d'Azur, IRD, Géoazur, 250 rue Albert Einstein, Sophia Antipolis 06560 Valbonne, France cardinal@geoazur-unice.fr*

*[2] Université Grenoble Alpes, Université Savoie Mont Blanc, CNRS, IRD, Université Gustave Eiffel, ISTerre, 38000 Grenoble, France*

*[3] Université Savoie Mont Blanc, CNRS, Pôle Montagne, Edytem, F-73370 Le Bourget-du-Lac, France*

*[4] Université Aix-Marseille, CNRS-IRD-Collège de France-INRAE, UM 34 CEREGE, Technopôle de l'Environnement Arbois-Méditerranée, BP80, 13545 Aix-en-Provence, France*

**ASTER Team: Georges Aumaître, Didier L. Bourlès†, Karim Keddadouche*

**ABSTRACT**

Fluvial incision is one of the major erosive processes acting at Earth's surface and is highly sensitive to tectonic, isostatic and climatic variations. The aim of this study is to distinguish between the short-term climatic fluctuations versus the long-term tectonic forcing contribution to Late-Quaternary fluvial incision, to better understand its timing and driving mechanism(s). To achieve this goal, we measured in situ-produced $^{36}$Cl concentrations along several river-polished gorge walls in Jurassic limestones of the Southwestern Alps. We then compared our dating results to previously-dated river gorges from nearby catchments. This allows us to highlight three trends of distinct incision dynamics, and to discuss their relationships with climate and tectonics. Trend 1 shows the direct impact of a paraglacial crisis in the rivers directly connected to glaciated areas. Trend 2 suggests an incision wave propagating along the non-glaciated tributaries following enhanced incision in the main

streams. Trend 3 displays steady and low incision rates in gorges disconnected from any fluvial response to glacier retreat. Trend 3 also seems to highlight the potential of resistant lithologies to isolate portions of the river network from post-glacial incision propagation. Our analysis shows that gorges connected to upstream glaciers exhibit a significant response of fluvial incision to climatic fluctuations, evidenced by high-amplitudes incision rate variations hindering the long-term tectonic signal. In contrast, incision rates inferred from disconnected gorges are in agreement with previously-estimated long-term denudation and rock-uplift rates in the area. Based on the latter, we can conclude that Late-Quaternary river incision in the Southwestern Alps is readjusting to both short-term climatic forcing and long-term tectonic forcing.

**Keywords**: River gorges; Quaternary; Fluvial incision; $^{36}$Cl dating; Southwestern Alps

## 1. INTRODUCTION

The morphology of mountainous landscapes is the result of a dynamic balance between erosion/sedimentation and uplift/subsidence (Penck, 1924; Hack, 1960; Willett, 1999; Whipple, 2001; Lavé and Avouac, 2001; Willett et al., 2002). As one of the major erosive processes acting at the Earth's surface, fluvial incision is highly sensitive to vertical motions linked to the isostatic response of the lithosphere or to tectonic forces (England and Molnar, 1990; Howard et al., 1994; Lavé and Avouac, 2001; Wobus et al., 2006), and to external forcing mainly represented by climatic fluctuations and associated base-level changes (Bacon et al., 2009; Pan et al., 2003; Van der Woerd et al., 2002; Ferrier et al., 2013).

Fluvial incision can be used as a first-order proxy for quantifying such dynamic processes over $10^4$-$10^5$ yr timescales. Indeed, in a perfectly balanced system between uplift and erosion, the quantification of fluvial incision allows direct estimate of the mean uplift (Royden and

Perron, 2013). However, this can only be valid if rivers processes and longitudinal profiles have reached steady-state conditions (Molnar and England, 1990; Burbank et al., 1996; Whipple, 2001; Whipple and Tucker, 1999), which has only been demonstrated in few areas (e.g. Cyr and Granger, 2008; Lavé and Avouac, 2001).

Although this hypothesis may be valid over long time scales ($10^5$-$10^6$ yr), fluvial incision rates often fluctuate over shorter time scales ($10^3$-$10^4$ yr) as they respond to climatic fluctuations (Pratt et al., 2002; Saillard et al., 2014; Rolland et al., 2017). Indeed, the erosive potential of rivers is principally controlled by the amount of water runoff and transported sediments within the drainage network (Seild and Dietrich, 1992; Whipple et al., 2000; Lague et al., 2005; Stock et al., 2005; DiBiase and Whipple, 2011), which can be enhanced through extreme and punctuated events such as floods, landslides or glacial outbursts (Tucker and Whipple, 2002; Pratt et al., 2002; Holm et al., 2004; Korup and Schlunegger, 2007; Gran et al., 2013; Lebrouc et al., 2013). The occurrence of these events is directly linked to climatic variations, especially in mountainous areas like the European Alps, where the conditions had been wetter and warmer during interglacial periods (Brocard et al., 2003; Bigot-Cormier et al., 2005; Sanchez et al., 2010, Zerathe et al., 2014). In addition, and over longer time scales, Plio-Quaternary glaciations have shaped the Alpine valleys and topography through cyclic fluctuations between glacial and interglacial periods (van der Beek and Bourbon, 2008; Brocard et al., 2003; Norton et al., 2010; Valla et al., 2011; Fox et al., 2015) and have led to a drastic increase in erosion rates and sedimentation fluxes from the internal reliefs to the surrounding basins (Hinderer, 2001; Kuhlemann et al., 2002; Champagnac et al., 2007; Herman and Champagnac, 2016).

While catchment-scale approaches have commonly been used to estimate average erosion rates (e.g. Bierman and Steig, 1996), few studies have focused on more local features such as Alpine headwalls (Mair et al., 2019) or bedrock fluvial gorges (Schaller et al., 2005; Ouimet

et al., 2008). Some of these studies have been carried out to quantify local fluvial incision rates on different catchments from the Southwestern (SW) French Alps, where bedrock gorges walls have been dated by Cosmic Ray Exposure (CRE) dating methods (e.g. Saillard et al., 2014; Rolland et al., 2017; Petit et al., 2017; 2019). These studies demonstrated a strong relationship between the onset of fluvial incision and the post-LGM (Last Glacial Maximum, i.e. after ca. 20 ka) glacial retreat, pointing towards the climatic transition from glacial to interglacial conditions as the main factor for controlling the postglacial incision and evolution of these valleys. However, none of these studies was able to quantitatively disentangle the respective contribution of climatic forcing and long-term tectonic uplift in the fluvial incision signal.

Indeed, isolating the respective contributions from tectonics and climate to mountain erosion is challenging (Herman et al., 2013), especially in this context where studied rivers are still possibly in disequilibrium, triggered by the recent glacial imprint on the topography (Norton et al., 2010), thus obscuring any potential long-term tectonic signal.

Based on these observations and current knowledge gaps, the major questions addressed in this work are the following:

- What is the driving mechanism for bedrock gorge incision after the LGM in the SW Alps?
- What is the relative contribution of short-term climatic fluctuations vs. long-term tectonic forcing in the observed fluvial incision rates in the SW Alps?

In the following, we present new CRE dating from five bedrock gorges in the Bès, Verdon, Paillon and Roya rivers catchments, distributed from the western to the eastern sides of the SW Alpine foreland (Figure 1). These five sites where chosen to complement the previously-acquired CRE dating dataset in foreland catchments disconnected from LGM ice-extent (e.g. Petit et al., 2019; Cardinal et al., 2021), in order to document incision rates at the

scale of the entire SW Alps. To quantify incision rates, we dated fluvially-polished limestone bedrock gorges with in situ-produced $^{36}Cl$. We then compared these new data with previously-published results with the aim to (1) discuss the timing and spatial variations in fluvial incision across the SW External Alps and (2) identify the major factors (climate vs. tectonics) that controlled fluvial incision dynamics over the last ca. 30 kyr.

## 2. STUDY AREA

### 2.1. Geological and tectonic settings

The studied area is located in the French Southwestern Alps (Figure 1A), where mountain building results from Cenozoic Alpine collision between European and African (Apulian) plates. The shortening of the European foreland has led to the exhumation of the crystalline basement (External Crystalline Massif or ECM) by crustal-scale thrusting (Nouibat et al. 2022) and fold and thrust belt propagation in the sedimentary foreland (Jourdon et al., 2014). In the SW Alps, the sedimentary cover is decoupled from the basement and transported by the Digne thrust sheet prolonged in the SE by the Arc of Castellane (Figure 1B). This fold-and-thrust belt is undergoing uplift and erosion due to the late implication of basement in the shortening. In this context, the Argentera ECM has been uplifted since 20 Ma (Lickorish & Ford, 1998; Sanchez et al., 2011) (Figure 1B). At the front of the Digne thrust, the sedimentary cover has been carved by an erosional window since 5 Ma (Schwartz et al., 2017). The folding of the sedimentary cover produces at the surface alternation between resistant rock bars, corresponding to the Tithonian (Upper Jurassic) limestone, and low-resistance lithologies, corresponding to the middle-late Jurassic “Terres Noires” marls and Cretaceous limestone-marl alternations.

Regarding to the present-day tectonic setting of the Alps, studies have shown a slow and complex deformation pattern in a global strike-slip context related to the rotation of Apulian plate (Mathey et al., 2021; Piña-Valdés et al., 2022). In this context, the internal part of the

Alps has been subjected to extensional deformation since 3 Ma, whereas its external part still undergoes compression (Sue et al., 1999; Bilau et al., 2020), as shown by geodesy and seismicity (Walpersdorf et al., 2018; Mathey et al., 2021; Piña-Valdés et al., 2022). This deformation pattern is characterized by a shortening rate of ≤1 mm/yr (Nocquet et al., 2016) and vertical component culminating in the ECMs with rates > 1mm/yr (Serpelloni et al., 2013).

### 2.2. Late-Quaternary Alpine climatic variations

The last major glaciation in the European Alps culminated during the Last Glacial Maximum (LGM; 26.5-19 ka; Clark et al., 2009). The LGM had a huge impact on the SW Alpine relief by enhancing and focusing erosion (Darnault et al., 2012). It was followed by a period of rapid glacial retreat (Clark et al., 2009), which is evidenced in the high-elevation areas of the Argentera massif by glacier thinning at 19-18 ka, followed by a major retreat of glaciers at elevations > 2500 m by ca. 14.5 ka (Darnault et al., 2012; Brisset et al., 2015; Rolland et al., 2019), similar to other observations at the scale of the European Alps (Ivy Ochs et al., 2008; Rea et al., 2020). Although Federici et al. (2012) dated moraines at 20 ka on the Italian side of the Southwestern Alps, the maximal glacial extent during the LGM is still not well constrained on the French side due to the lack of preservation of frontal moraines in the low-elevation valley floors (Figure 1C; Julian, 1980; Brisset et al. 2015). A later and spatially limited glacial re-advance occurred at ca. 12 ka during the Younger Dryas (Hinderer, 2001; Heiri et al., 2014), which rapidly receded at 11-10 ka (Federici et al., 2008; Darnault et al., 2012; Wanner et al., 2015).

The Holocene started at about 11.7 ka with a transition to warmer climatic conditions (Wanner et al., 2011, 2015). Climatic reconstructions during the Holocene can be problematic because both the timing and magnitude of the warming vary substantially between different regions (Renssen et al., 2009). However, Wanner et al. (2011) proposed a division of the

present interglacial into three climatic periods: (1) a deglaciation phase immediately following the end of the Younger Dryas cold phase and characterized by important ice melting; (2) the 'Holocene Thermal Optimum' between 11 and 5 ka (Wanner at al., 2008, Renssen et al., 2009, 2012), characterized by a warmer and more stable climate, and (3) a 'Neoglacial' period, with colder conditions and higher precipitations during the late-Holocene (Davis et al., 2003). These climatic variations can play a major role for the erosion processes including river incision in zones of high lithological contrasts (Petit et al., 2019).

**2.3. Study sites**

In this study, we present new data acquired from five gorges located in the French Southwestern Alps (Figure 1C). The Pérouré Gorge is located in the Bès catchment, a tributary of the Durance River. The High Verdon Gorge is formed by the Verdon River, which is also a tributary to the Durance River. The Redebraus Gorge is located in the Paillon catchment, which reaches the Mediterranean Sea in the city of Nice. The Bévéra and Bendola gorges are located along the eponym rivers, which are tributaries to the Roya River catchment located along the southern France-Italy border. All the studied catchments feature strong lithological contrasts which, combined with the widespread folding of the region, create significant convexities and slope breaks in the longitudinal river profiles. Indeed, all the above-mentioned gorges are incised in Tithonian limestones, which occur repeatedly in the Alpine Foreland and is surrounded by less resistant marls, and form strong lithological knickpoints along longitudinal river profiles (Figure 2).

Together with published data, this new dataset allows us to distinguish three gorge dynamics according to their geographical location and regarding the ice-covered domains during the LGM (Figure 1C):

- Connected: the gorge site is located on a main stream that takes its source in the previously LGM ice-covered part of the catchment;

- Indirectly-connected: the gorge is located along a tributary of a connected main stream;
- Disconnected: the gorge is located along a catchment that was devoid of any glacier and along a stream with no, direct nor indirect, connection to ice-covered areas.

The Verdon River is considered as 'connected', as its upper catchment belongs to the LGM glaciated areas. The Bendola, Bévéra and the Bès Rivers are 'indirectly-connected' to glaciations, because they are tributaries of main rivers that have their sources in previously glaciated areas. The Paillon River on the other hand had no glaciers in its catchment, and can therefore be considered as totally "disconnected" from any significant glacial extension during the LGM (Figure 1C). In order to compare our data with previous results, we also selected previously-sampled limestone bedrock gorges "indirectly-connected" (Esteron Gorge, Petit et al., 2019; and Barles Gorge, Cardinal et al., 2021) and connected (Courbaisse Gorge, Rolland et al., 2017; Vésubie Gorge, Saillard et al., 2014) from the literature (Figure 1C).

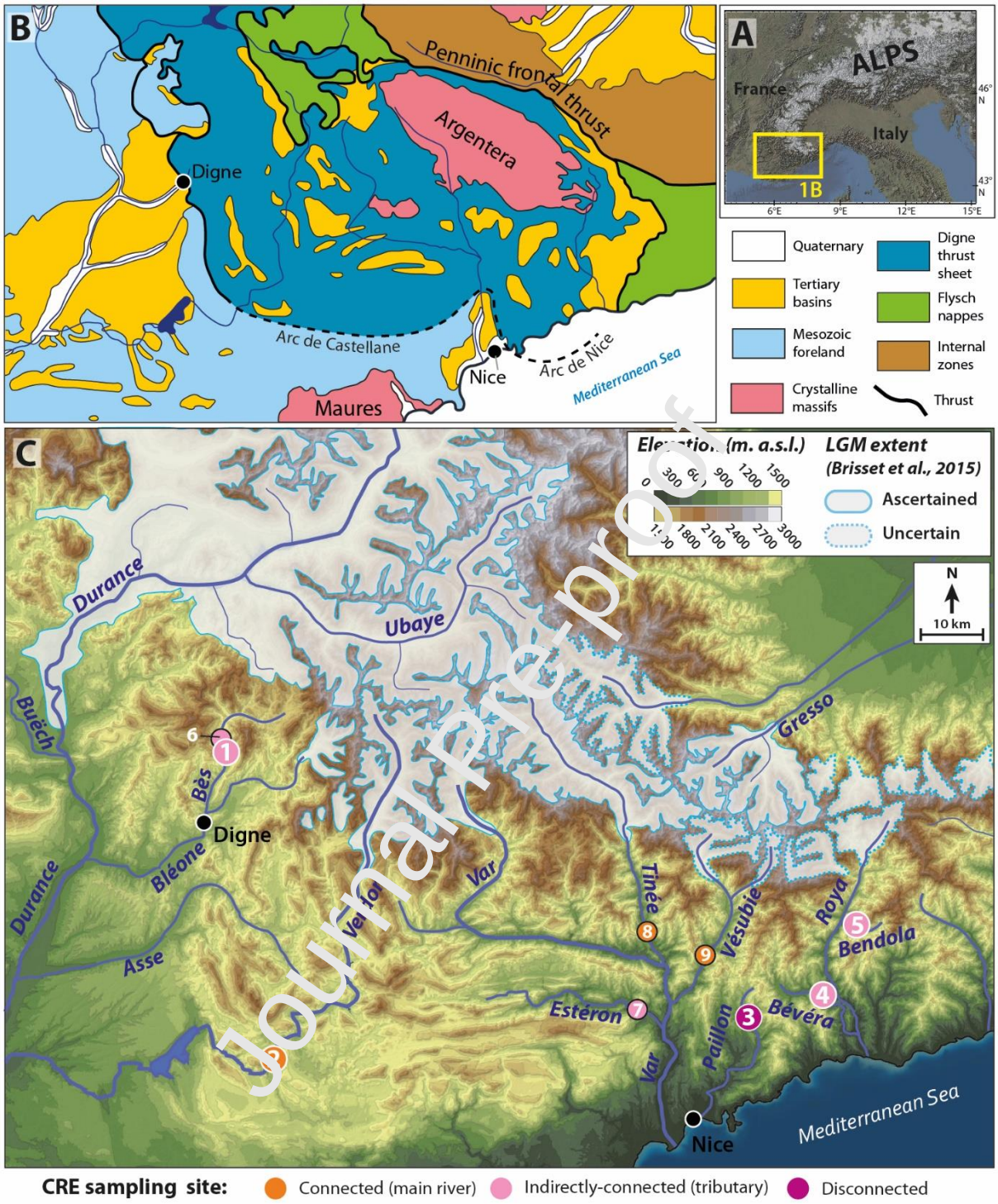


Figure 1. A: Location of study area in the European Alps. B: Southwestern Alps general tectonic framework (modified after Schwartz et al., 2017). C: Location of the Pérouré (1), High Verdon (2), Redebraus (3), Bévéra (4) and the Bendola (5) gorges from this study (white wider circles) and previously dated sites from literature (black circles): (6) Clue de Barles (Cardinal et al., 2021); (7) Estéron (Petit et al., 2019); (8) Courbaisse (Rolland et al., 2017);

(9) Vésubie (Saillard et al., 2014). The grey area shows the Last Glacial Maximum (LGM) glacier extent (modified from Brisset et al., 2015).

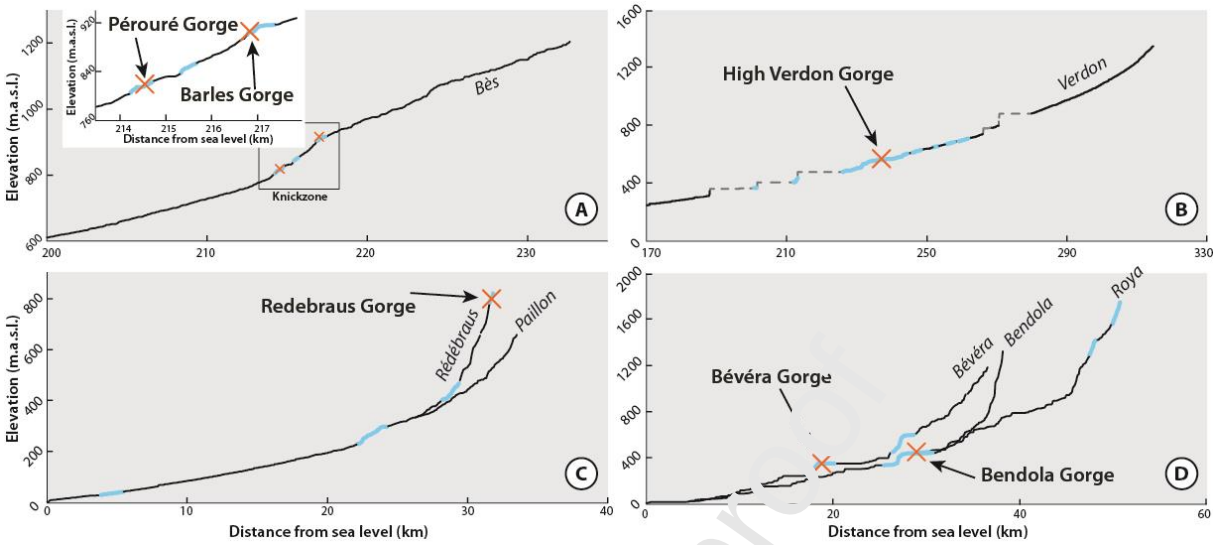


Figure 2. Longitudinal profiles of the sampled rivers and their main stream. A: Bès River, with a blow-up on a knickzone and the location of two sampled gorges (Pérouré, this study, and Barles, Cardinal et al., 2021); B: Verdon River; C: Paillon Rive and the tributary Redebraus; D: Roya River and the tributaries Bévéra and Bendola. Sampling sites are indicated with a red cross; location of outcropping massive Tithonian limestones along the channels are indicated by a thick blue line. Dashed grey lines correspond to artificial lakes (dams) along the Verdon River. The distance from sea level correspond to the distance from the river mouth to the Mediterranean Sea.

## 3. METHODS

### 3.1. $^{36}$Cl CRE dating method

In this study, we used in situ-produced cosmogenic $^{36}$Cl measurements to constrain exposure ages along the flanks of the five studied bedrock gorges incised into resistant limestone lithologies.

#### 3.1.1. Sampling strategy and field work

We aim at quantifying gorge incision rates along steep (almost vertical) bedrock walls that were theoretically gradually exposed as the river incised (Schaller et al., 2005; Ouimet et

al., 2008). We can therefore expect a distribution of younger to older CRE ages from the current riverbed level to the top of the bedrock gorge walls. Sampled surfaces were chosen based on the following morphological indices: i) evidence of preservation of an induration varnish or with low apparent superficial dissolution, indicating little weathering since exposure or ii) presence of smooth river-polished surfaces and "pot holes", representing polished and concave fluvial erosional surfaces preserved in the gorge walls (Figure 3 and 4) and iii) with no overhanging relief and located in the most opened part of their respective gorges, in order to maximize exposure to cosmic rays.

Our main goal was to find and sample a continuous wall of polished limestone bedrock. In addition, we sampled, when possible, two facing walls along the same gorge (Figure 3C, E and 4B) as well as abandoned flat erosional surfaces above to the sampled walls (Figure 3D). Although we strived to collect sample as close to the river bed as possible, as it has been done in the Redebraus and Benevola Gorges (Figure 3D, E and 4B), stream depth and strong currents have sometimes prevented us from reaching the lower part of the gorge. The selected profiles are also shorter than 15 m to avoid any influence of potential rock-falls, which may cause the rejuvenation of the gorge wall surface, as demonstrated by Cardinal et al. (2021). Samples were gathered using a drill, hammer and chisel. In total, a number of 61 limestone samples have been collected (Table 1).

### 3.1.2. Analytical protocol

We prepared the bulk limestone samples at the 'Laboratoire National des Nucléides Cosmogéniques' (LN2C; CEREGE, Aix-en-Provence) following the procedure presented in Schimmelpfennig et al. (2009). $^{36}$Cl concentrations were determined by accelerator mass spectrometry (AMS) performed on ASTER, the French national AMS facility (CEREGE, Aix-en-Provence) (Arnold et al., 2010). All measurements were calibrated against in-house CEREGE SM-CL-12 standard (Merchel et al., 2011). Total uncertainties account for counting

statistics, standard evolution during measurements, standard uncertainty and external uncertainties of 2.74%, 2.13% and 1.62 % for $^{36}Cl/^{35}Cl$, $^{36}Cl/37Cl$ and $^{35}Cl/^{37}Cl$ ratios, respectively (Braucher et al., 2018). A sea-level and high-latitude $^{36}Cl$ production rate for calcium spallation of 42.2±3.4 atoms $^{36}Cl\ g^{-1}\ a^{-1}$ (Schimmelpfennig et al., 2009, Braucher et al., 2011) has been used and scaled following Stone (2000) and corrected for topographic shielding (TS), constrained from field measurement data. $^{36}Cl$ ages have been determined using the approach of Schimmelpfennig et al. (2009) using a limestone density of 2.6 g $cm^{-3}$.

### 3.2. Incision rate quantification

We used the code developed by Glotzbach et al. (2011) originally designed for thermochronology data, to define best-fitting line segments passing through the CRE data points, in order to determine incision rate variations with time from our data and literature data. We made some modifications to the code in order to make it more suitable for CRE age data. As in Glotzbach et al. (2011) we used a Monte-Carlo approach to randomly split the data into 1, 2 or 3 successive time intervals in order to define line segments by weighted linear regression, and select the best-fitting ones according to their $R^2$ value. We have implemented the following criteria: no negative incision rate is allowed, thus solutions containing segments with negative incision rates are discarded; line segments constrained by less than 3 data points are discarded; the intersection between two line segments must correspond to the intersection between the two groups of data that were used to compute them (so that there is no data point that is used to compute a line segment, but lies outside of its boundaries).

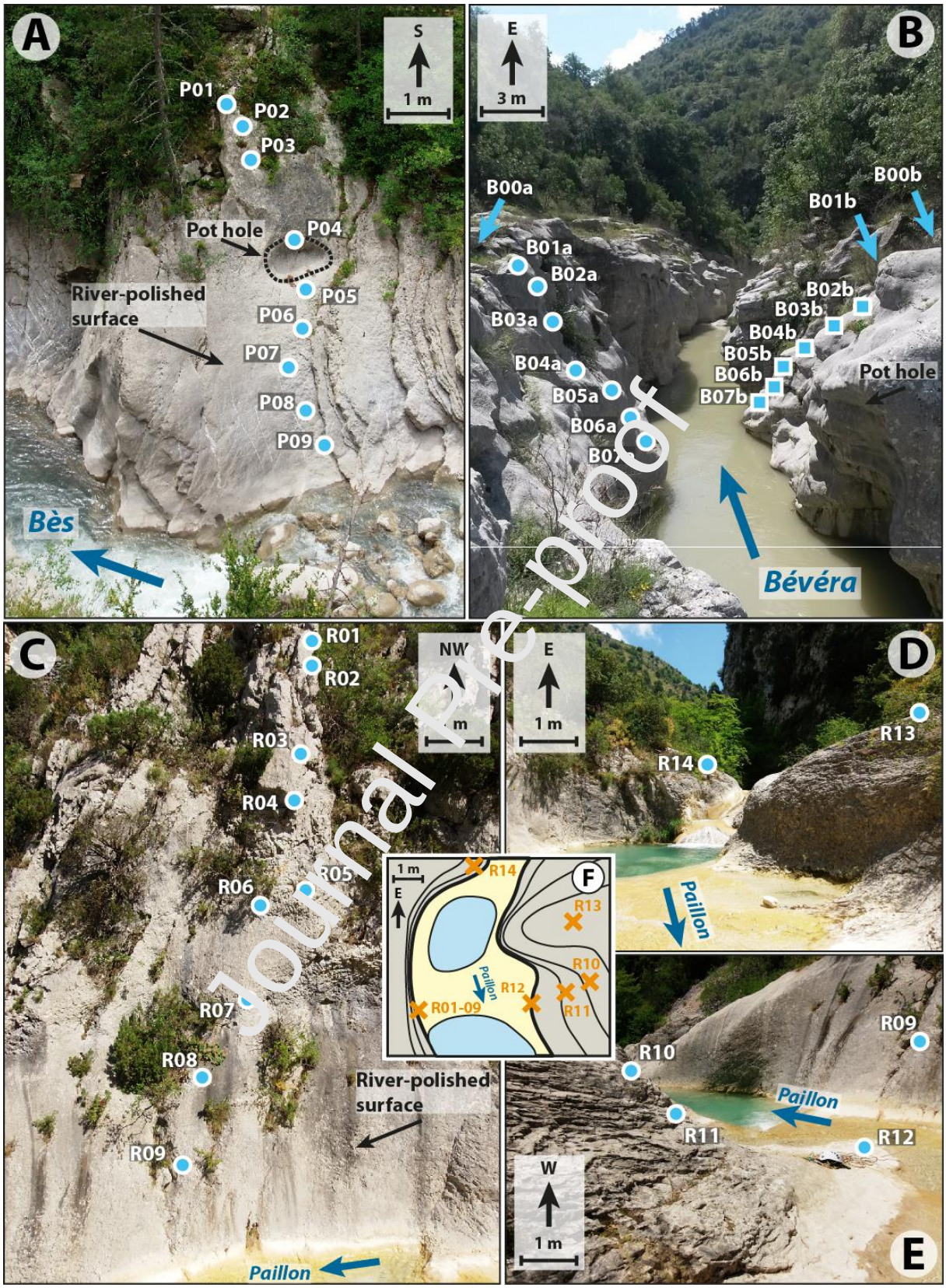


Figure 3. Sampling sites in the (A) Pérouré Gorge, (B) northern (circles) and southern (squares) flanks of the Bévéra Gorge and (C, D and E) Redebraus Gorge. The inset (F) locates the different sampled surfaces in the Redebraus Gorge.

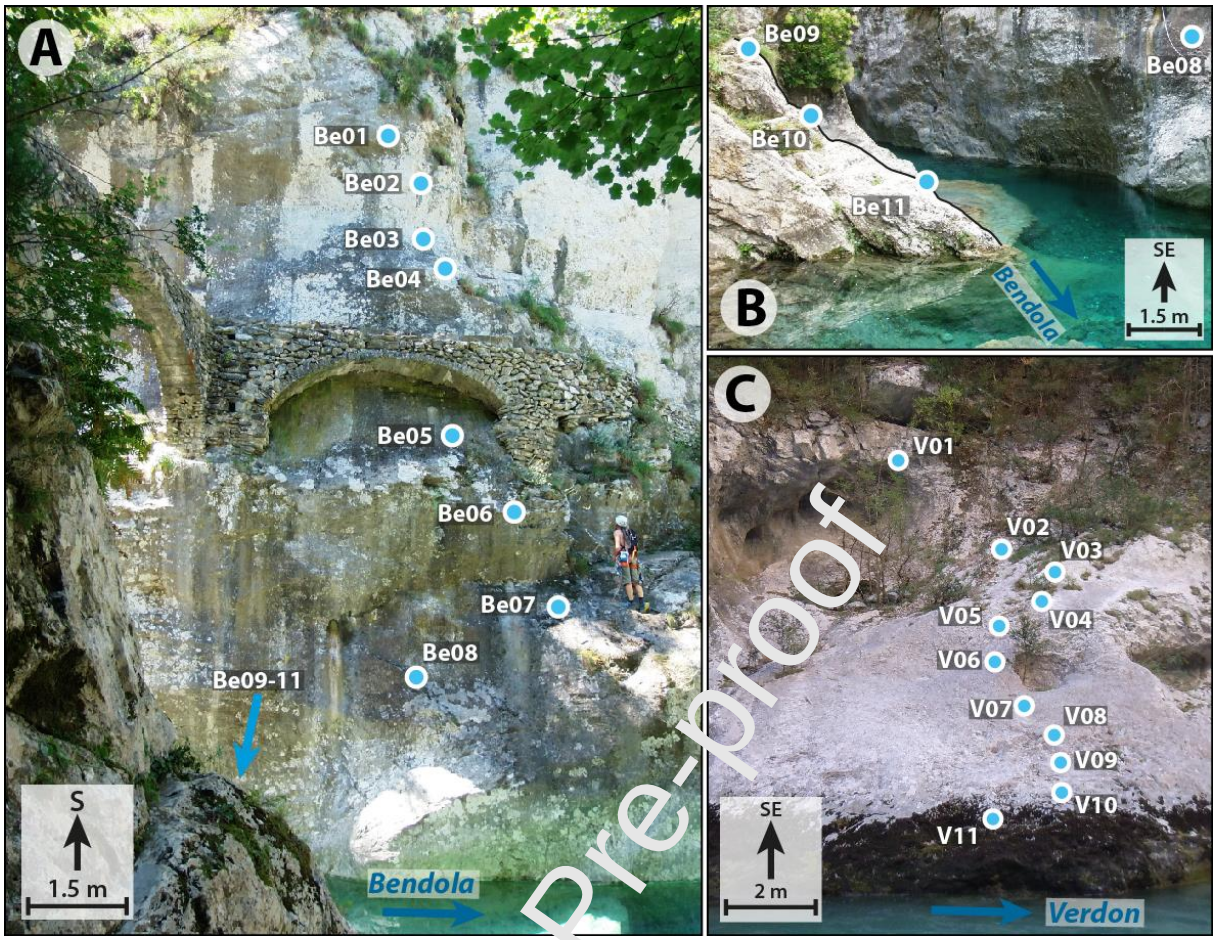


Figure 4. Sampling sites and samples location in the Bendola Gorge (A, B) and the High Verdon Gorge (C)

## 4. $^{36}$Cl CRE DATING RESULTS

### 4.1. New $^{36}$Cl CRE dating results in the SW French Alps

For the five studied gorges, CRE ages determined from $^{36}$Cl concentrations are reported in the age-elevation plots (green circles; Figure 5), with the corresponding regression lines (black lines). From these data, we estimated the mean incision rate (blue lines), with the corresponding uncertainty envelope (grey envelopes), which are shown in the same plot for each site.

The nine limestone samples gathered from the Pérouré Gorge (Figure 3A) display ages ranging between ca. 1 and 9 ka (Table 1). From these ages, we can compute two mean incision rates: a first, poorly-constrained (regarding the $R^2$) incision rate of 0.76±0.11 mm/yr

from 3 ka to 9 ka (from 11 to 6 meters above riverbed level), with a $R^2$ of 0.47, and a second, better constrained value of 3.34±0.88 mm/yr from 1 ka to 3 ka (from 1 to 6 meters above riverbed level), with a $R^2$ of 0.73.

The eleven $^{36}$Cl CRE ages obtained along a polished surface of the High Verdon Gorge range from 15 ka to 40 ka. From these ages, we can estimate a steady incision rate of 0.21±0.01 mm/yr, from 15 to 45 ka, with a $R^2$ of 0.97. Two samples (V01 and V02; Table 1) are discarded as it seems that their exposure ages are related to post-incision rejuvenation of the bedrock wall, which is most likely representative of rock-fall occurrences (Figure 4C).

Fourteen limestone samples were collected along a 15 m high vertical wall in the Redebraus Gorge. From the sample $^{36}$Cl concentrations, we obtained CRE ages ranging between 6 and 84 ka, giving a steady mean incision rate of 0.21±0.03 mm/yr with a $R^2$ of 0.85. In this data set, two samples (R03 and R05; Table 1) are not taken into account for the incision-rate computation, as their exposure ages are probably related to a rock-fall event that occurred at ca. 20 ka (Figure 3C, D, E, F).

The sixteen samples gathered in the Bévéra Gorge display CRE ages between 19 and 5 ka (Table 1). From these ages, we can compute a mean incision rate increasing from 0.52±0.15 mm/yr, between 20 and 10 ka (with a $R^2$ of 0.68), to 0.84±0.51 mm/yr, from 10 to 5 ka , (with a $R^2$ of 0.73, Figure 3B).

In the Bendola Gorge, the CRE ages of eleven carbonate samples ranges between 5 and 44 ka. The mean incision rate is estimated at 0.28±0.04 mm/yr during this period, with a $R^2$ of 0.88. On this profile, two samples (Be01 et Be02; Table 1) are considered as outliers and therefore not taken into account for the incision rate computation. Indeed, their young exposure ages, compared to the ages of the surrounding samples, and their location, seems to indicate a post-incision rejuvenation of the bedrock walls (Figure 4A, B).

### 4.2. $^{36}$Cl CRE dating results from literature

In order to interpret our data in a more regional framework, we propose here a compilation of CRE dating studies that have been previously carried out on bedrock gorges and valleys at the scale of the SW Alps (Saillard et al., 2014; Rolland et al., 2017; Petit et al., 2019; Cardinal et al., 2021; Figure 1). In order to compare the results with our data, we re-computed the previously estimated incision rates with the same method as in this study (Figure 6). We chose to use only the CRE data considered by the authors as suitable for deriving fluvial incision rates. The data considered as outliers, for reasons such as rock-falls, are not presented in this study.

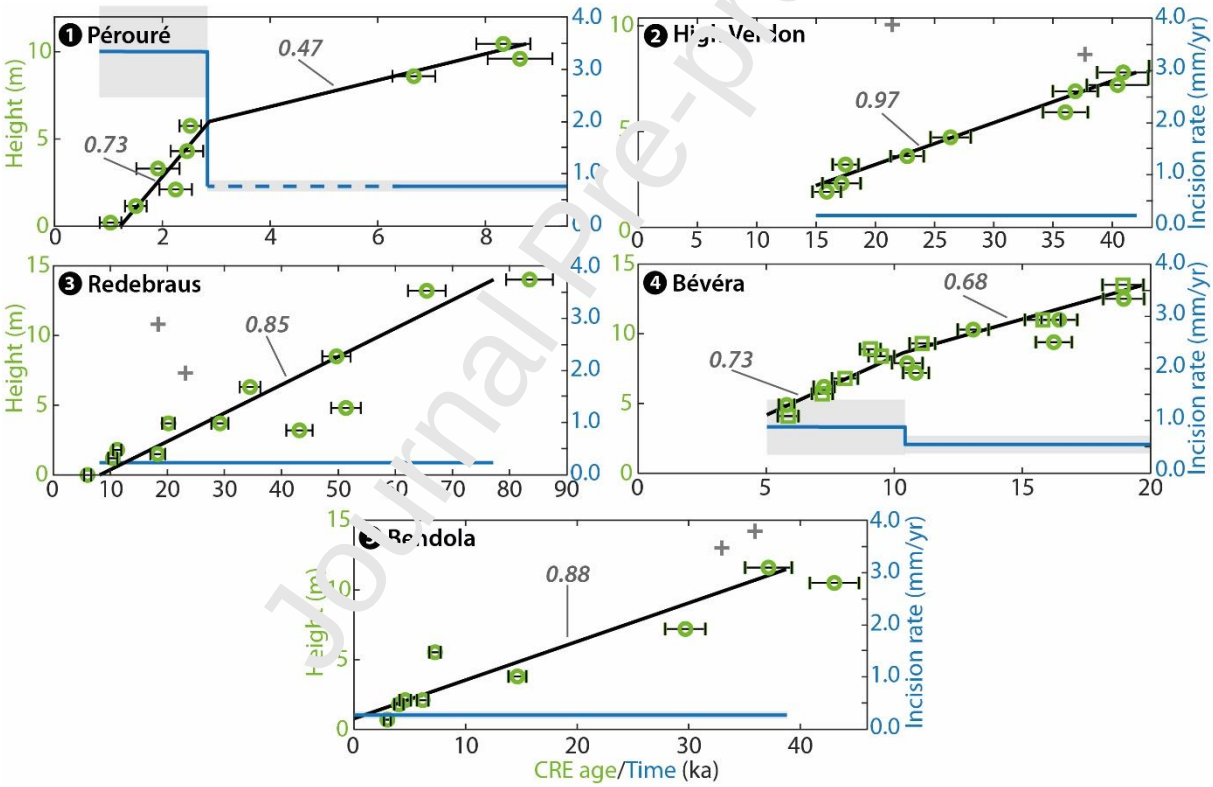


Figure 5. CRE age vs height (green circles) and corresponding regression (black line, with $R^2$ value); mean incision rate (blue line) throughout time, with uncertainty (grey envelope), plot of the gorges (1) Pérouré; (2) High Verdon; (3) Redebraus; (4) Bévéra, and (5) Bendola, from this study. The blue dashed line for Pérouré (plot 1) corresponds to the temporal range where the estimate of incision rate is poorly constrained, due to a lack of data and low $R^2$. The

number of each plot refers to the location of sites displayed in Figure 1C. The grey crosses are outliers considered as representing rejuvenation of the gorge walls following a rock-fall event and are therefore not representative of fluvial incision.

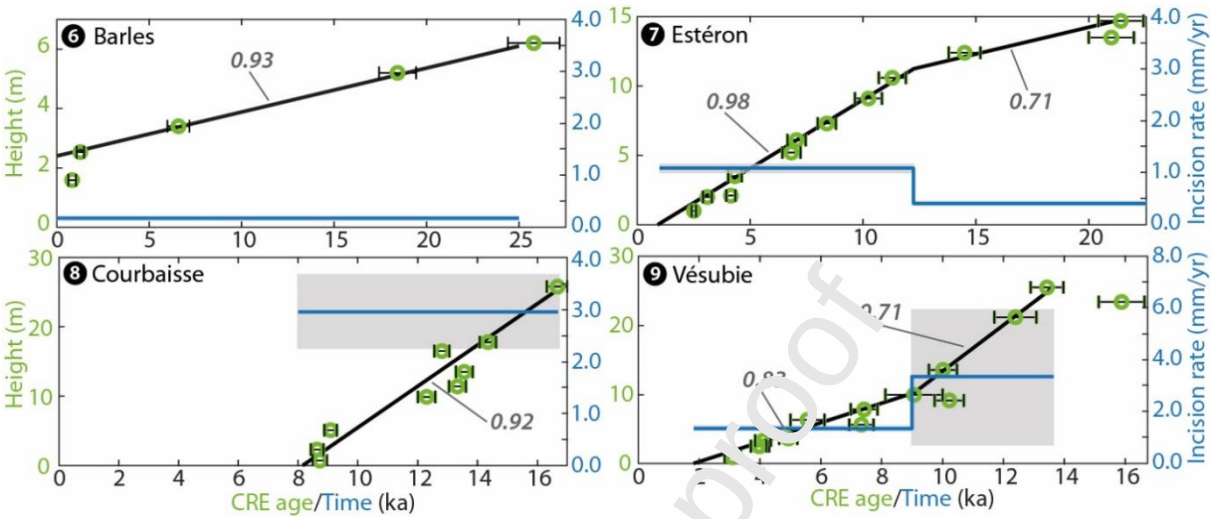


Figure 6. CRE age vs height (green circles) and corresponding regression (black line, with $R^2$ value); mean incision rate (blue line) throughout time, with uncertainty (grey envelope), of the gorges from literature: (6) Clue de Barles (Cardinal et al., 2021); (7) Estéron (Petit et al., 2019); (8) Courbaisse (Rolland et al., 2017); (9) Vésubie (Saillard et al., 2014). Data have been selected based on the authors interpretation of the sampled surfaces as representative of exposure related to fluvial incision.

| Sample | Height above river (m) | TS factor | Spall. scaling | $^{35}$Cl (ppm) | Ca (%) | Atoms $^{36}$Cl (at/g) | Atoms $^{36}$Cl ± (at/g) | CRE age (ka) |
|---|---|---|---|---|---|---|---|---|
| **Pérouré Gorge** (lat: 44.2°; long: 6.3°; elevation: 814 m.a.s.l.) | | | | | | | | |
| P01 | 11.2 | 0.71 | 1.44 | 34.8 | 37.4 | 225855 | 14252 | 8.3±0.5 |
| P02 | 10.3 | 0.71 | 1.44 | 48.4 | 38.0 | 244501 | 18207 | 8.6±0.6 |
| P03 | 9.3 | 0.71 | 1.44 | 48.0 | 39.2 | 192883 | 13705 | 6.7±0.4 |
| P04 | 6.5 | 0.71 | 1.44 | 36.3 | 37.8 | 70483 | 5823 | 2.5±0.2 |
| P05 | 5.0 | 0.71 | 1.44 | 36.0 | 38.2 | 68158 | 7821 | 2.5±0.3 |
| P06 | 4.0 | 0.71 | 1.44 | 40.0 | 36.9 | 51295 | 11467 | 1.9±0.4 |
| P07 | 2.8 | 0.71 | 1.44 | 37.9 | 38.0 | 60377 | 8918 | 2.2±0.3 |
| P08 | 1.9 | 0.71 | 1.44 | 38.3 | 37.6 | 40900 | 6808 | 1.5±0.2 |
| P09 | 0.9 | 0.71 | 1.44 | 30.8 | 32.1 | 25038 | 3868 | 1.0±0.2 |
| **High Verdon Gorge** (lat: 43.8°; long: 6.4°; elevation: 606 m.a.s.l.) | | | | | | | | |
| *V01* | *11* | *0.16* | *1.67* | *24.5* | *40.4* | *110890* | *8575* | *21.6±1.7* |
| *V02* | *8* | *0.16* | *1.67* | *33.1* | *40.6* | *190457* | *16417* | *37.3±3.2* |

| | | | | | | | | |
|---|---|---|---|---|---|---|---|---|
| V03 | 7.7 | 0.16 | 1.67 | 23.4 | 40.7 | 205909 | 11192 | 40.9±2.2 |
| V04 | 7.1 | 0.16 | 1.67 | 28.6 | 40.8 | 205363 | 13024 | 40.4±2.6 |
| V05 | 6.8 | 0.16 | 1.67 | 28.1 | 40.8 | 187869 | 9775 | 36.9±1.9 |
| V06 | 5.8 | 0.16 | 1.67 | 32.0 | 41.7 | 188287 | 9862 | 36.0±1.9 |
| V07 | 4.6 | 0.16 | 1.67 | 31.5 | 40.6 | 136006 | 8988 | 26.4±1.7 |
| V08 | 3.7 | 0.16 | 1.67 | 35.0 | 40.7 | 118596 | 7068 | 22.7±1.4 |
| V09 | 3.3 | 0.16 | 1.67 | 32.5 | 40.8 | 91776 | 5730 | 17.5±1.1 |
| V10 | 2.4 | 0.16 | 1.67 | 29.9 | 40.7 | 89670 | 8452 | 17.2±1.6 |
| V11 | 2 | 0.16 | 1.67 | 37.3 | 40.7 | 83944 | 6349 | 15.9±1.2 |
| **Redebraus Gorge** (lat: 43.8°; long: 7.4°; elevation: 527 m.a.s.l.) | | | | | | | | |
| R01 | 14.0 | 0.42 | 1.58 | 18.86 | 40.1 | 946227 | 46163 | 83.5±4.1 |
| R02 | 13.2 | 0.42 | 1.58 | 19.22 | 41.3 | 778602 | 39778 | 65.5±3.3 |
| *R03* | *10.5* | *0.42* | *1.58* | *14.97* | *39.1* | *559664* | *29727* | *18.9±1.0* |
| R04 | 8.5 | 0.42 | 1.58 | 15.10 | 39.0 | 568296 | 28656 | 49.7±2.5 |
| *R05* | *7.1* | *0.42* | *1.58* | *19.14* | *40.1* | *280560* | *14695* | *23.1±1.2* |
| R06 | 6.3 | 0.42 | 1.58 | 20.16 | 40.3 | 416307 | 21504 | 34.5±1.8 |
| R07 | 4.8 | 0.30 | 1.58 | 19.78 | 41.5 | 449910 | 22703 | 51.3±2.6 |
| R08 | 3.2 | 0.30 | 1.58 | 18.82 | 41. | 374066 | 19766 | 43.2±2.3 |
| R09 | 1.5 | 0.30 | 1.58 | 18.96 | 41.8 | 165956 | 11664 | 18.3±1.3 |
| R10 | 1.83 | 0.64 | 1.58 | 20.91 | 41.0 | 214946 | 14291 | 11.2±0.7 |
| R11 | 1.2 | 0.64 | 1.58 | 21.78 | 41.2 | 201575 | 15016 | 10.4±0.8 |
| R12 | 0.0 | 0.64 | 1.58 | 22.74 | 41.3 | 117198 | 12115 | 6.0±0.6 |
| R13 | 3.7 | 0.64 | 1.58 | 23.23 | 41.1 | 551920 | 28682 | 29.2±1.5 |
| R14 | 3.7 | 0.64 | 1.58 | 21.35 | 40.8 | 381736 | 20217 | 20.2±1.1 |
| **Bévéra Gorge** (lat: 43.9°; long: 7.5°; elevation: 281 m.a.s.l.) | | | | | | | | |
| B00a | 12.5 | 0.89 | 1.27 | 11.3 | 37.8 | 380994 | 16676 | 19.0±0.8 |
| B01a | 11.0 | 0.89 | 1.27 | 11.4 | 37.9 | 331854 | 15069 | 16.4±0.7 |
| B02a | 10.3 | 0.80 | 1.27 | 18.9 | 37.9 | 243162 | 10644 | 13.1±0.6 |
| B03a | 9.4 | 0.63 | 1.27 | 12.4 | 38.0 | 231557 | 10194 | 16.2±0.7 |
| B04a | 7.9 | 0.56 | 1.27 | 12.4 | 37.9 | 134514 | 8034 | 10.5±0.6 |
| B05a | 7.2 | 0.56 | 1.27 | 21.1 | 37.8 | 143352 | 7200 | 10.9±0.5 |
| B06a | 6.2 | 0.66 | 1.27 | 17.1 | 37.8 | 111662 | 5721 | 7.3±0.4 |
| B07a | 4.9 | 0.64 | 1.27 | 16.1 | 37.8 | 85610 | 4754 | 5.8±0.3 |
| B00b | 13.5 | 0.81 | 1.27 | 15.4 | 38.0 | 351203 | 14916 | 18.9±0.8 |
| B01b | 11.0 | 0.81 | 1.27 | 33.4 | 37.7 | 310241 | 13924 | 15.8±0.7 |
| B02b | 9.3 | 0.75 | 1.27 | 12.9 | 37.9 | 190555 | 8637 | 11.1±0.5 |
| B03b | 8.9 | 0.69 | 1.27 | 15.9 | 38.0 | 144324 | 7151 | 9.1±0.4 |
| B04b | 8.4 | 0.62 | 1.27 | 16.0 | 37,9 | 136508 | 6619 | 9.5±0.5 |
| B05b | 6.8 | 0.54 | 1.27 | 12.9 | 38.0 | 100400 | 5648 | 8.1±0.5 |
| B06b | 5.7 | 0.48 | 1.27 | 17.2 | 38.0 | 78976 | 4716 | 7.0±0.4 |
| B07b | 4.1 | 0.48 | 1.27 | 19.1 | 37.9 | 66429 | 4192 | 5.9±0.4 |
| **Bendola Gorge** (lat: 44.0°; long: 7.5°; elevation: 357 m.a.s.l.) | | | | | | | | |
| *Be01* | *14.2* | *0.32* | *1.35* | *40.9* | *40.3* | *284628* | *15689* | *35.1±1.9* |
| *Be02* | *13.0* | *0.32* | *1.35* | *42.8* | *40.3* | *262445* | *14997* | *32.2±1.8* |
| Be03 | 11.6 | 0.32 | 1.35 | 34.1 | 41.0 | 303029 | 16727 | 37.2±2.1 |
| Be04 | 10.5 | 0.32 | 1.35 | 29.3 | 40.9 | 346005 | 18060 | 43.1±2.2 |
| Be05 | 7.2 | 0.32 | 1.35 | 62.4 | 41.4 | 254491 | 15799 | 29.8±1.8 |
| Be06 | 5.6 | 0.62 | 1.35 | 17.4 | 40.9 | 117113 | 7733 | 7.3±0.5 |

| | | | | | | | | |
|---|---|---|---|---|---|---|---|---|
| Be07 | 3.8 | 0.62 | 1.35 | 51.4 | 41.1 | 243041 | 14049 | 14.7±0.8 |
| Be08 | 2.1 | 0.62 | 1.35 | 39.0 | 41.0 | 101697 | 7463 | 6.2±0.5 |
| Be09 | 2.1 | 0.62 | 1.35 | 41.5 | 40.5 | 75596 | 8545 | 4.6±0.5 |
| Be10 | 1.8 | 0.62 | 1.35 | 45.9 | 40.5 | 66751 | 6722 | 4.0±0.4 |
| Be11 | 0.7 | 0.62 | 1.35 | 67.8 | 41.0 | 51873 | 5002 | 3.0±0.3 |

Table 1. $^{36}$Cl CRE sample characteristics and geochronological results. Sample field information, natural chlorine, calcium, cosmogenic $^{36}$Cl contents in the limestone samples, resulting $^{36}$Cl CRE ages, and topographic shielding (TS) factor of the sampled surfaces, are indicated. Samples written in italics correspond to the CRE ages identified as outliers and discarded for incision rate computation.

## 5. DISCUSSION

### 5.1. Synthesis of $^{36}$Cl CRE dating results for bedrock gorges in the SW Alps

From the synthesis of CRE datings of gorges in the SW Alps, we are able to highlight different spatial and temporal patterns of bedrock gorge incision rates at a regional scale. Two orders of information emerged from the plot of incision rate variations through time (Figure 7A): (i) the differences in incision rate magnitude from one site to another, and (ii) the temporal variations of incision rates for each individual site. From these observations, we can distinguish three distinct trends (Figure 7A):

- The first trend (Trend 1, green lines) shows a high incision rate (~3 mm/yr) between 17 and 8 ka. The concerned gorges (Courbaisse #10 and Vésubie #12) are located along "Connected" rivers.
- The second trend (Trend 2, orange lines) shows initially lower (~0.5 mm/yr) incision rates that increase up to 1 mm/yr after 10 ka. The concerned gorges (Bévéra, Estéron and Pérouré) are located along "Indirectly-connected" tributaries.
- The third trend (Trend 3, blue lines) shows steady and lower incision rates at around 0.25 mm/yr, from 80 ka to the present day. The concerned gorges (Barles, High Verdon, Rédébraus and Bendola) have mixed locations regarding the LGM extent.

Most of the studied gorges show significant change in incision rates around 10 kan while

four sites do not undergo any changes in their incision rate since up to 80 ka. Incision rate increase occurs before 10 ka for Trend 1 and later for Trend 2. These variations will be discussed in the following section.

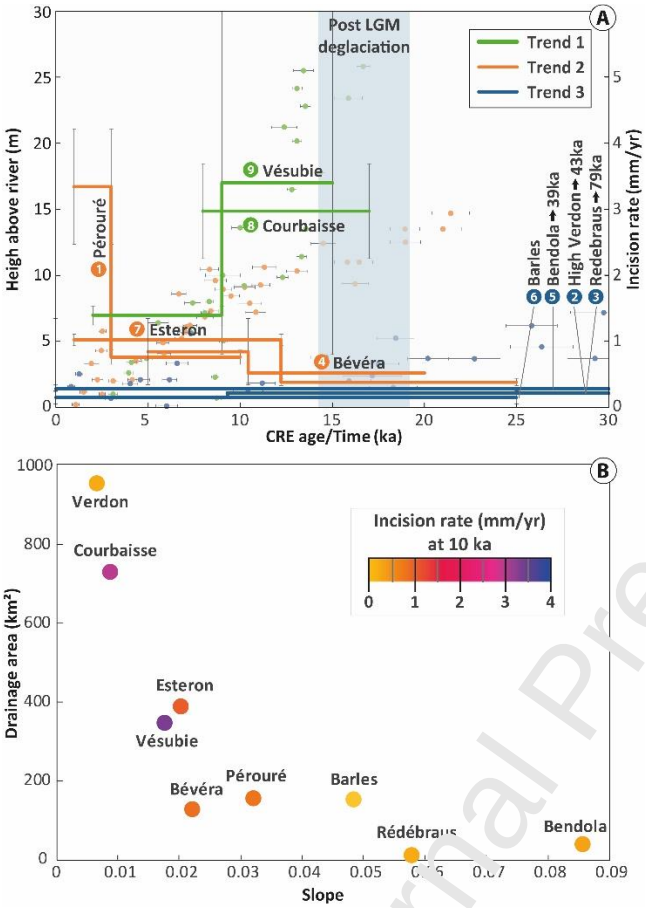


Figure 7. A, Incision rate trends (Trend 1 to 3) in SW Alps gorges, constrained by $^{36}$Cl exposure ages; individual dots correspond to dated samples (left vertical axis) and lines to the corresponding incision rate (right vertical axis). Note that the plot only displays data since 30 ka. Bendola, High Verdon and Redebraus gorges ages show a similar incision rate extending up to 39, 43 and 79 ka respectively, as indicated. B, Upstream drainage area versus local slope plot of sampled SW Alps bedrock gorges, with corresponding mean incision rates (color scale) estimated at 10 ka.

### 5.2. **Regional pattern of river incision rates in SW Alps and their relationship to lithology, climate and uplift**

Comparison of incision rates obtained from several catchments at the scale of the SW Alps is not straightforward, as fluvial incision is influenced by local factors like stream and catchment morphologies. Before addressing any regional interpretation of the obtained incision patterns, it is crucial to take into account some local features, such as upstream drainage area, local slope and rock erodibility, which control the incision efficiency (e.g., Kirby and Whipple, 2012). We tested the hypothesis that variations in drainage area, which is considered as a proxy of river discharge and sediment flux (Bishop et al., 2005), and in local slope could explain the measured differences in incision rates from one gorge to another. Both variables are co-dependent to the position of a considered point along the river profile: the more upstream this point is, the higher the slope and the smaller the drainage area (e.g., Wobus et al., 2006). We choose incision rates at 10 ka in order to compare our incision data with present-day catchments metrics. Our analysis (Figure 7B) shows this expected decreasing exponential relationship between upstream drainage area and channel slope. As these two parameters control the incision, we would expect, when comparing incision rates from gorges with their respective catchment metrics, to find higher incision rates for both high slope and drainage area sector. However, although there is a group of high incision rates (Bévéra, Vésubie, Péroure, Estéron) for intermediate slopes and drainage areas, no clear tendency emerges from this plot: both high and low incision rates are recorded either for large and small drainage areas and similarly for high and low local slopes. . This analysis suggests that other factors could explain the different trends of incision rates highlighted in Figure 7A, which are discussed below.

### 5.3. **Trend 1: direct deglaciation impact**

Trend 1 (green lines, Figure 7A), which includes data from Courbaisse (Rolland et al., 2017) and Vésubie (Saillard et al., 2014) gorges, shows a mean incision rate of ~3 mm/yr between 17 and 8 ka, which decreases to 1.4 mm/yr for the Vésubie Gorge and appears to

become null in Courbaisse Gorge after ca. 10 ka (Figure 7A). During this period, the SW Alps were under the influence of climatic fluctuations, with a transition period from full glacial (LGM) to interglacial (after 10 ka) conditions (e.g. Ivy Ochs et al., 2008). Direct erosion by glaciers is known to be very efficient in the shaping of the Alps (Champagnac et al., 2007; Valla et al., 2011; Sternai et al., 2013). Indeed, during the LGM, the erosion rate in the Argentera ECM has been estimated at 1.8 mm/yr by Darnault et al. (2012). The sampled gorges of Vésubie and Courbaisse are located in formerly-glaciated catchments, downstream and outside of the LGM glacial extent. Furthermore, fluvial incision occurred in these gorges since at least the end of the LGM, when main glaciers were retreating. This time marks the beginning of the paraglacial period (Church and Ryder, 1972), which is characterized by enhanced fluvial processes, such as increased stream flow (Seidl and Dietrich, 1992; Tucker and Whipple, 2002) and increased sediment yield (Ballantyne, 2002; Meigs et al., 2006; Savi et al., 2014). Church and Ryder (1972) proposed a theoretical paraglacial model, in which the sediment yield peaks shortly after the onset of deglaciation and decreases until reaching a steady state, after paraglacial sediment supply exhaustion. Although additional processes (discussed below) may control the apparent stop of incision in the Courbaisse Gorge, the CRE dating data displayed by Trend 1 could fit with the theoretical paraglacial model (Church and Ryder, 1972; Ballantyne, 2002), which seems to illustrate the consequence of increased sediment yield from upstream Tinée and Vésubie catchments between the end of the LGM (ca. 19 ka) and the Younger Dryas/Holocene transition (ca. 10 ka).

While it is commonly assumed that sediment yield/discharge plays an important role in bedrock incision process (Seild and Dietrich, 1992; Whipple et al., 2000; Stock et al., 2005; DiBiase and Whipple, 2011), the direct relationship between incision and sediment supply is more complex (Sklar and Dietrich, 2001; Whipple and Tucker, 2002). Indeed, sediment

transported by rivers can both provide the tools for bedrock incision, through abrasion or plucking process, and, if excessively profuse, can insulate and protect the underlying riverbed from erosion (Sklar et Dietrich, 2001). The apparent ceasing of incision in the Courbaisse Gorge, observed in the CRE data (Figure 6A) may be controlled by the cover effect. Indeed, the gorge is located in a much more opened part of the Tinée valley, where hillslope-derived sediment seems to have filled the bottom of the valley, impeding the bedrock incision.

Our results suggest continuous incision during the Late glacial period (19-11ka), that we associated with increased sediment yield. Similarly, Van den Berg et al. (2012) quantified present-day incision rate of 1.3 mm/yr and proposed post LGM incision rates of 2.1-2.8 mm/yr to explain the formation of inner-gorges in the Emme Catchment (Switzerland), which suggests a similar pattern at the scale of the Alpine belt. It is worth noting that sediment yield in the Var basin (Bonneau et al., 2017) and denudation rates in the Argentera ECM (Mariotti et al., 2021) estimated from marine sediment records show two peaks since 30 ka: a major one at the end of the LGM and a secondary one at ca. 10 ka. Between these two periods, both studies of Bonneau et al. (2017) and Mariotti et al. (2021) reported a decrease in sediment yield and apparent denudation rates respectively. The discrepancy between these studies and ours might be the result of transient sediment storage, either on land, at the mouth of the Var River, or on the submarine slope (Petit et al., submitted). .

### 5.4. **Trend 2: indirect deglaciation impact**

Trend 2 (orange lines, Figure 7A), which includes data from Esteron (Petit et al., 2019), Bévéra and Pérouré (this study) gorges, shows incision rates of ~ 0.5 mm/yr that increase up to ~ 1 mm/yr after 10 ka. While we see the influence of deglaciation in rivers that are directly connected to formely-glaciated areas, we can observe an acceleration of incision after 10 ka in rivers that are tributaries of these “Connected” rivers, and thus indirectly connected to glaciations (Figure 1C). This acceleration could be related to the propagation of

an incision wave in tributaries, whose local base level at the outlet dropped, as the main river underwent a paraglacial crisis and associated profile re-equilibration(Figure 8, top). The possible control of a regional base level is not considered here because no significant drop of the Mediterranean Sea level has been observed since the end of LGM (Vacchi et al., 2016; Benjamin et al., 2017).

If we follow this hypothesis, the paraglacial incision pulse in the main rivers should have started after 17 ka (i.e., corresponding to the onset of fast incision in connected rivers of Trend 1). Yet, the incision acceleration in "Trend 2" gorges appears to be delayed by more than 5 ka with respect to "Trend 1" ones. Although several authors have proposed that post-glacial incision may be delayed after deglaciation by several thousands of years (Valla et al., 2010; Jansen et al., 2011), this delay could also be controlled by the distance between the sampled gorge and the tributary confluence to the main stream, that the climatic knickpoint had to incise through while migrating upstream. Indeed, the Estéron gorge is located ~7km upstream from its junction with the Var River, while the Bévéra Gorge is located ~15 km upstream from its junction from the Roya River, and our data show that incision rate increases earlier in the Estéron Gorge (ca. 12 ka) than in the Bévéra Gorge (ca. 10 ka). Regarding the Pérouré Gorge, the data are too scarce to discuss further any possible propagation of incision between 10 and 15 ka (Figure 7A).

Several other factors can be invoked to explain this variation in the onset of fast incision from one river to another, such as sediment availability, water discharge and bedrock resistance. Besides, we do not find any indication of upstream migration of knickpoints along the tributary river profiles, but only static lithological knickpoints formed in the most resistant limestone strata. The latter will be discussed in more detail in the following section.

### 5.5.Lithological control on incision propagation

We proposed from Trends 1 and 2 that the location of the sampled gorges, with respect to

LGM ice-covered extension (connected or indirectly-connected), controls the processes and rates at which the incision occurs. However, the gorges included in Trend 3 do not belong to a single domain regarding the glacier coverage. Indeed, the High Verdon Gorge was connected to glaciers, while Barles and Bendola gorges were indirectly connected. Those three gorges display very similar incision rates (0.15-0.28 mm/yr) to the Rédébraus Gorge (0.21±0.03 mm/yr), although the latter is the only one that is totally disconnected from any glacial influence. Therefore, it seems that these gorges have not been impacted by deglaciation and did not undergo any significant post-glacial incision.

We argue here that bedrock resistance plays a major role in the distribution and propagation of erosion in a fluvial system, as observed in previous studies (e.g. da Silva Guimarães et al., 2021). The notion of bedrock resistance here is relative to the lithology of one unit compared to another. In this study, we compare mainly the resistance of thick Tithonian limestone bars to known less resistant marl lithologies that are widespread in underlying and overlying strata. The Bès River example seems to illustrate this effect. Along this tributary, that is connected to the Bléone River, we sampled the Pérouré Gorge, just less than 2 km downstream of previously sampled Barles Gorge (Cardinal et al., 2021). From these two gorges, we can observe significant differences in incision rates. The Pérouré Gorge shows an overall higher incision rate (0.76±0.11 mm/yr), with an apparent increase at 4 ka (3.34±0.88 mm/yr), while the Barles Gorge displays a steady incision rate of 0.15±0.03 mm/yr. When looking at the Bès River long profile (Figure 2A), we see that the two gorges are located at both ends of a knickzone, in which we see three lithological knickpoints formed at each Tithonian limestone outcrop. This example could highlight the role of a strong bedrock lithology as a barrier partly impeding upstream incision propagation, as demonstrated by several studies (Crosby and Whipple, 2006, Jansen et al., 2010, Bishop and Goldrick, 2010). Considering this effect, we suggest that the upstream migration of a post-glacial

incision wave is able to pass through the first knickpoint, but significantly decreases and even disappears as it migrates upstream through the knickzone towards Barles Gorge (Figure 8, bottom, T1)

The Roya catchment case could also reflect the control of lithology, in which we sampled two tributaries: the Bévéra and the Bendola. As in the Bévéra River, we would expect an acceleration of incision related to knickpoint propagation along the Bendola River, which would have occurred earlier as the Bendola Gorge is located within less than 1 km from its junction with the Roya River. When looking at the longitudinal river profiles (Figure 2D), we see that the outlet of the Bendola River is located along an outcrop of Tithonian limestone, and slightly upstream of the lips of the knickpoint formed in this resistant lithology, whereas the Bendola outlet is located in a much less resistant lithology (Middle Jurassic marls). We thus propose that the Bendola River did not undergo any significant base level drop as a result of the paraglacial crisis in the Roya River and therefore was not subject to any upstream knickpoint propagation, as opposed to the Bévéra River (Figure 8, bottom, T2).

Regarding the High Verdon Gorge case, it seems that the gorge did not undergo any post-glacial incision rate change, as opposed to the Vésubie or Courbaisse gorges. The Verdon longitudinal river profile (Figure 2B) presents a concave profile, especially upstream of the High Verdon Gorge. The lithology upstream of the Tithonian limestone in which the gorge is incised, is mainly composed of lower-resistance marls. The easily erodible lithology, in addition to the steady-state river profile could have dampened the impact of a paraglacial incision wave coming from the upstream glaciated area, located more than 50 km upstream. In addition to this effect, the position of the gorge more than 70 km upstream from the confluence with the Durance River could have prevented the High Verdon Gorge from undergoing any significant knickpoint propagation.

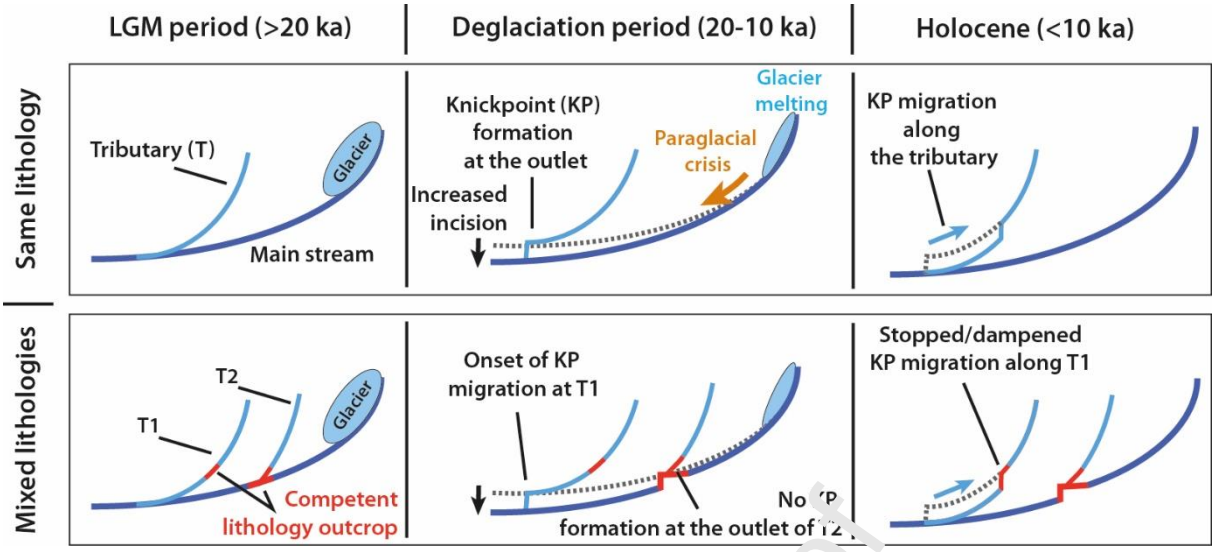


Figure 8. Top: Theoretical sketch of tributary readjustment to a change of base level following paraglacial crisis in the main river with homogenous lithology. Bottom: Theoretical sketch of the impact of mixed lithologies (limestones/marls) on the incision propagation and tributary readjustment to a change of base level following paraglacial crisis in the main river.

### 5.6. Trend 3: steady-state

Trend 3, which includes data from Barles (Cardinal et al., 2021), High Verdon, Redebraus and Bendola (this study) gorges shows a slow and steady mean incision rate of ~0.25 mm/yr since maximum 80 ka. The main remaining question is: what drives these steady and lower incision rates displayed in Trend 3?

The climatic influence is shown through punctual and very efficient incision pulses, which can hinder any lower and longer-term signal. Therefore, to better understand such low incision rates we must integrate our data in a larger time window, where short-term climatic influence will be smoothed. Incision rates inferred from these isolated gorges seem comparable to previously-determined long-term erosion rates. Based on the CRE dating of alluvial terraces in the Buëch river (Figure 1C), Brocard et al. (2003) deduced a long-term (190 ka) incision rate of about 0.8 mm/yr. Based on bulk sediment cosmonuclides ($^{10}$Be) concentration, Mariotti et al. (2021) obtained catchment-average denudation rates ranging from 0.1 to 1.4 mm/yr since 75 ka in the Var River catchment (Figure 1C).

Under steady-state conditions, erosion rate is believed to match rock uplift rate (Royden and Perron, 2013). Long-term exhumation rates obtained from the external crystalline massifs to the foreland are of the order of 0.3-1.4 mm/yr. In the Argentera ECM (Figure 1B), cooling rates estimated by low-temperature thermochronology (Apatite fission track and Apatite U-Th/He dating), are in agreement with exhumation rates of 0.8-1.4 mm/yr over the last 10 Ma (Bogdanoff et al., 2000; Bigot-Cormier et al., 2006; Sanchez et al., 2011). In the Frontal domain, Apatite (U-Th/He) dating on basin sediments had shown a reset induced by the Digne thrust sheet (Figure 1B) and returns exhumation rates of around 0.7 mm/yr since 5 Ma (Schwartz et al., 2017). East of the city of Nice, Bigot-Cormier et al. (2004) analysed seismic-reflection profiles to infer uplift rates of 0.3-0.5 mm/yr of the North Ligurian margin since 5 Ma. Regarding the present-day uplift, several studies using GPS data in the Alps (Serpelloni et al., 2013; Nocquet et al., 2016; Walpersdorf et al., 2018; Sternai et al., 2019; Piña-Valdés et al., 2022) evidence limited to slow vertical displacements of <0.5 mm/yr in the SW Alps.

Although, these values encompass different time scales, from long-term (10 Ma) to short-term (>100 a) and show a large variability, Trend 3 mean incision rates estimated at about of ~0.25 mm/yr in Trend 3 seem in agreement with those slow uplift rates. Therefore, our data could indicate that incision process within these disconnected (from glacier) or isolated river gorges is a response to a steady base-level drop induced by tectonically-driven rock uplift.

## 6. CONCLUSION

In conclusion, our $^{36}$Cl CRE dating of incised bedrock gorges seems to highlight three different incision rate trends in the Southwestern Alps:

- Trend 1, in which connected gorges seem to have undergone an increase, directly after the LGM, followed by a decrease of incision. We propose that the variations in the recorded incision rates could firstly be related to an increase in the sediment yield and then to the depletion of sediment, commonly associated with the paraglacial period.

- Trend 2, with gorges affected by a small increase in incision rates after the deglaciation that could reflect the propagation of an erosion wave in tributaries of connected rivers.
- Trend 3, apparently unaffected by the last glacial-interglacial period, as suggested by the observed slow and steady incision rates (~0.25 mm/yr since maximum 80 ka). These values are similar to long-term erosion rates and in the range of the modern vertical GPS displacements.

As well as potentially highlighting the control of resistant lithology on incision propagation within river catchments, these observations, although based on a limited number of sites, provide insights for discussing the influence of different forcings (climate and tectonics) in the SW Alps. In locations significantly affected by late-Quaternary glaciers, the influence of climate is shown through the direct and indirect impact of deglaciation. There, the associated high gorge incision rates could hinder the lower and longer-term tectonic signal. Indeed, when out of the glacial influence, river incision rates are comparable to long-term (> 10 Ma) erosion rates. Therefore, our results and interpretations suggest that Late-Quaternary river incision in the Southwestern Alps is readjusting to both short-term climatic forcing and long-term tectonic forcing.

**ACKNOWLEDGMENTS**

This study has been funded by the French Geological Survey (Bureau de Recherches Géologiques et Minières; BRGM) through the national program “Référentiel Géologique de France” (RGF-Alpes). This work has been supported by the French government, through the UCA-JEDI Investments in the Future project managed by the National Research Agency (ANR) with the reference number ANR-15-IDEX-01. The $^{36}$Cl measurements were performed at the ASTER AMS national facility (CEREGE, Aix en Provence) which is supported by the INSU/CNRS, the ANR through the "Projets thématiques d’excellence"

program for the "Equipements d'excellence" ASTER-CEREGE action and IRD. The authors thank Myette Guiomar and the Réserve Géologique de Haute Provence for their support during field work. This manuscript benefitted from constructive reviews from Fritz Schlunegger and an anonymous reviewer who are thanked for their comments and suggestions.

**REFERENCES CITED**

Arnold M., Merchel S., Bourlès D.L., Braucher R., Benedetti L., Finkel R.C., Aumaître G., Gottdang A. and Klein M., 2010. The French accelerator mass spectrometry facility ASTER: improved performance and developments. Nucl. Instrum. Methods Phys. Res., B 268, 1954–1959.

Bacon S.N., McDonald E.V., Caldwell T.G. et Dalldorf G.K., 2009. Timing and distribution of alluvial fan sedimentation in response to strengthening of late Holocene ENSO variability in the Sonoran Desert, southwestern Arizona, USA. Quaternary Res., 73, 425-438.

Ballantyne C.K., 2002. A general model of paraglacial landscape response. The Holocene, 12, 3, 371-376.

Beck, C., Deville, E., Blanc, E., Philippe, Y., and Tardy, M., 1998. Horizontal shortening control of Middle Miocene marine siliciclastic accumulation (Upper Marine Molasse) in the southern termination of the Savoy Molasse Basin (northwestern Alps/southern Jura). Geol. Soc. Spec. Publ., 134, 263–278.

Benjamin J., Rovere A., Fontana A., Furlani S., Vacchi M., Inglis R. H., Galili E., Antonioli F., Sivan D., Miko S., Mourtzas N., Felja I., Meredith-Williams M., Goodman-Tchernov B., Kolaiti E., Anzidei M. and Gehrels R., 2017. Late Quaternary sea-level changes and early human societies in the central and eastern Mediterranean Basin: An interdisciplinary review. Quat. Int., 449, 29-57.

Bierman P. and Steig E.J., 1996. Estimating rates of denudation using cosmogenic isotope abundances in sediment. Earth Surf. Process. Landf., 21, 2, 125–139.

Bigot-Cormier F., Sage F., Sosson M., Déverchère J., Ferrandini M., Guennoc P., Popoff M. and Stéphan J.-F., 2004. Déformations pliocènes de la marge nord-Ligure (France) : les conséquences d'un chevauchement crustal sud-alpin. Bull. Soc. géol. Fr., 175, 2, 197-211.

Bigot-Cormier F., Braucher R., Bourlès D., Guglielmi Y., Dubar M. and Stéphan J.-F., 2005. Chronological constraints on processes leading to large active landslides. Earth Planet. Sci. Lett., 235, 141-150.

Bilau A., Rolland Y., Schwartz S., Godeau N., Guihou A., Deschamps P., Brigaud B., Noret A., Dumont T. and Gautheron C., 2020. Extensional reactivation of the Penninic Frontal Thrust 3 Ma ago as evidenced by U-Pb dating on calcite in fault zone cataclasite. Solid Earth, 12, 1, 237-251.

Bishop P. and Goldrick G., 2010. Lithology and the evolution of bedrock rivers in post-orogenic settings: Constraints from the high elevation passive continental margin of SE Australia. Geological Society, London, Special Publications, 346, 267-287.

Bogdanoff S., Michard A., Mansour M. and Poupeau G., 2000. Apatite fission track analysis in the Argentera massif: evidence of contrasting denudation rates in the External Crystalline Massifs of the Western Alps. Terra Nova, 12, 117-125.

Bonneau L., Toucanne S., Bayon G., Jorry S. J., Emmanuel L. and Jacinto R. S., 2017. Glacial erosion dynamics in a small mountainous watershed (Southern French Alps): A source-to-sink approach. Earth Planet. Sci. Lett., 458, 366-379.

Braucher R., Merchel S., Borgomano J. and Bourlès D.L., 2011. Production of cosmogenic radionuclides at great depth : a multi element approach. Earth Planet. Sci. Lett., 309, 1-9.

Braucher R., Keddadouche K., Aumaître G., Bourlès D.L., Arnold M., Pivot S., Baroni M.,

Scharf A., Rugel G. and Bard E., 2018. Chlorine measurements at the 5 MV French AMS national facility ASTER: associated external uncertainties and comparability with the 6MV DREAMS facility. Nucl. Instrum. Methods Phys. Res., B 420, 40–45.

Brisset E., Guiter F., Miramont C., Revel M., Anthony E.J., Belhon C., Arnaud F., Malet E. and de Beaulieu J.-L., 2015. Lateglacial/Holocene environmental changes in the Mediterranean Alps inferred from lacustrine sediments. Quaternary Sci. Rev., 110, 49-71.

Brocard G.Y., Van Der Beek P., Bourlès D., Siame L. et Mugnier J.-L., 2003. Long-term fluvial incision rate and postglacial river relaxation time in the French Western Alps from $^{10}$Be dating of alluvial terraces with assessment of inheritance, soil developpement and wind ablations effects. Earth Planet. Sci. Lett., 209, 197-214.

Brocard G. and van der Beek P., 2006. fluence of incision rate, rock strength, and bedload supply on bedrock river gradients and valley-flat widths: Field-based evidence and calibrations from western Alpine rivers (southeast France). Geol. Soc. Am. Bull., 398, 101-126.

Brocklehurst S.H. and Whipple K.X., 2002. Glacial erosion and relief production in the Esatern Sierra Nevada, California. Geomorphology, 42, 1-24.

Burbank D.W., Leland J., Fielding E., Anderson R.S., Brozovic N., Reid M.R., et Duncan C., 1996. Bedrock incision, rock uplift and threshold hillslopes in the northwestern Himalayas. Nature, 379, 505-510.

Cardinal T., Audin L., Rolland Y., Schwartz S., Petit C., Zerathe S., Borgniet L., Braucher R., Nomade J., Dumont T., Guillou V. and ASTER team, 2021. Interplay of fluvial incision and rockfalls in shaping periglacial mountain gorges. Geomorphology, 381, 107665.

Champagnac, J.D., Molnar P., Andersion R.S., Sue C. and Delacou B., 2007. Quaternary erosion-induced isostatic rebound in the western Alps. Geol. Soc. Am. Bull., 35, 3, 195-

198.

Champagnac J.-D., van der Beek P., Diraison G. and Dauphin S., 2008. Flexural isostatic response of the Alps to increased Quaternary erosion recorded by foreland basin remnants, SE France. Terra Nova, 20, 213-220.

Church M. and Ryder J.M., 1972. Paraglacial sedimentation: A consideration of fluvial processes conditionned by glaciation. GSA Bulletin, 83, 3059-3072.

Clark P.U., Dyke A.S., Shakum J.D., Carlson A.E., Clark J., Wohlfarth B., Mitrovica J.X., Hostetler S.W. and McCabe A.M., 2009. The Last Glacial Maximum. Science, 325, 710-714.

Crosby B. T. and Whipple K. X., 2006. Knickpoint initiation and distribution within fluvial networks: 236 waterfalls in the Waipaoa River, North Island, New Zealand. Geomorphology, 82, 16-38.

da Silva Guimarães E., Delunel R., Schlunegger F., Akçar N., Stutenbecker, L. and Christl M., 2021. Cosmogenic and Geological Evidence for the Occurrence of a Ma-Long Feedback between Uplift and Denudation, Chur Region, Swiss Alps. Geosciences, 11, 339.

Darnault R., Rolland R., Rolland Y., Bourlès D., Revel M., Sanchez G. and Bouissou S., 2012. Timing of the last deglaciation revealed by receding glaciers at the Alpine-scale: impact on mountain geomorphology. Quaternary Sci. Rev., 3, 127-142.

Davis B.A.S., Brewer S., Stevenson A.C., Guiot J. and Data Contributors, 2003. The temperature of Europe during the Holocene reconstructed from pollen data. Quaternary Sci. Rev., 22, 1701-1716.

DiBiase R. and Whipple K.X., 2011. The influence of erosion thresholds and runoff variability on the relationships among topography, climate, and erosion rate. J. Geophys. Res., 116, F04036.

England P. and Molnar P., 1990. Surface uplift, uplift of rocks, and exhumation of rocks. Geology, 18, 1173-1177.

Federici P. R., Granger D. E., Pappalardo M., Ribolini A., Spagnolo M. and Cyr A. J., 2008. Exposure age dating and Equilibrium Line Altitude reconstruction of an Egesen moraine in the Maritime Alps, Italy. Boreas, 37, 245–253.

Federici P. R., Granger D. E., Ribolini A., Spagnolo M., Pappalardo M. and Cyr A. J., 2012. Last Glacial Maximum and the Gschnitz stadial in the Maritime Alps according to 10Be cosmogenic dating. Boreas, 41, 277–291.

Ferrier K.L., Huppert K. L. and Perron J.T., 2013. Climatic control of bedrock river incision. Nature, 496, 206-209.

Fox M., Leith K., Bodin T., Balco G. and Shuster D.L., 2015. Rate of fluvial incision in the Central Alps constrained throught joint inversion of detrital $^{10}$Be and thermochronometric data. Earth Planet. Sci. Lett., 411, 27-36.

Gidon M.,1997. Les chaînons subalpins au nord-est de Sisteron et l'histoire tectonique de la nappe de Digne. Géologie Alpine, 73, 23–57.

Glotzbach C., van der Beek P. A. and Spiegel C., 2011. Episodic echumation and relief growth in the Mont Blanc massif, western Alps from numerical modelling of thermochronology. Earth Planet. Sci. Lett., 304, 417-430.

Godard V., Hippolyte J.-C., Cushing E., Espurt N., Fleury J., Bellier O., Ollivier V. and the ASTER Team, 2020. Hillslope denudation and morphologic response to rock uplift gradient. Earth Surf. Dynam., 8, 221–243.

Haccard Y., Beaudoin B., Gigot P. and Jorda M., 1989. Carte géologique de France (1/50 000), feuille LA JAVIE (918). Orléans : Bureau de recherche géologiques et minières. Note explicative par Haccard Y., Beaudoin B., Gigot P. et Jorda M. (1989), 152 p.

Hack J.T., 1960. Interpretation of erosional topography in humid temperature regions. Am. J.

Sci., 258, A : 80-97.

Hallet B., 1996. Glacial quarrying: a simple theorical model. Ann. Glaciol., 22, 1-8.

Heiri O., Koinig K.A., Spötl C., Barrett S., Brauer A., Drescher-Schneider R., Gaar D., Ivy-Ochs S., Kreshner H., Luetscher M., Moran A., Nicolussi K., Preusser F., Schmidt R., Schoeneich P., Schwörer C., Sprafke T., Terhorst B. and Tinner W., 2014. Paleoclimate records 60-8 ka in the Austrian and Swiss Alps and their forelands. Quaternary Sci. Rev., 106, 186-205.

Herman F., Seward D., Valla P.G., Carter A., Kohn B., Willet S.D. and Ehlers T.A., 2013. Worldwide acceleration of mountain erosion under a cooling climate. Nature, 504, 423-426.

Herman F. and Champagnac J.-D., 2016. Plio-Quaternaire increase of erosion rates in mountain belts in response to climate change. Terra Nova, 28, 2-10.

Hinderer M., 2001. Late Quaternary denudation in the Alp, valley and lake filling and modern river loads. Geodinamica Acta, 14, 231-263.

Holm K., Bovis M. and Jakob M., 2004. The landslide repsonse of alpine basins to post-Little Ice Age glacial timing and retreat in southwestern British Columbia. Geomorphology, 57, 201-216.

Howard A.D., Dietrich W.E. and Seidl A., 1994. Modelling fluvial erosion on regional to continental scales. J. Geophys. Res.: Solid Earth., 99, B7, 13,971-13,986.

Ivy- Ochs S., Kerschner H., Reuther A., Preusser F., Heine K., Maisch M., Kubik P.W. and Schlüchter C., 2008. Chronology of the last glacial cycle in the European Alps. J. Quaternary Sci., 23, 559-573.

Jansen J. D., Codilean A. T., Bishop P. and Hoey T. B., 2010. Scale Dependence of Lithological Control on Topography: Bedrock Channel Geometry and Catchment Morphometry in Western Scotland. The Journal of Geology, 118, 3, 223-246.

Jansen D. J., Fabel D., Bishop P., Xu S., Schnabel C. and Codilean A. T., 2011. Does decreasing paraglacial sediment supply slow knickpoint retreat? Geology, 39, 6, 543-546.

Jourdon A., Rolland Y., Petit C. and Bellahsen N., 2014. Style of Alpine tectonic deformation in the Castellane fold-and-thrust belt (SW Alps, France): Insights from balanced cross-sections. Tectonophysics, 633, 143-155.

Julian M., 1980. Les Alpes franco-italiennes, Etude Geomorphologique. Aix-Marseille Universitée.

Kirby, E. and Whipple, K.X., 2012. Expression of active tectonics in erosional landscapes. Journal of Structural Geology, 44, 54-75.

Korup O. and Schlunegger F., 2007. Bedrock landsliding, river incision, and transience of geomorphic hillslope-channel coupling: evidence from inner gorges in the Swiss Alps. J. Geophy. Res., 112, F03027.

Kuhlemann J., Frisch W., Székely B., Dunkl I. and Kázmér M., 2002. Postcollisional sediment budget history of the Alps: Tectonic versus climatic control. Int. J. Earth Sci., 91, 818–837.

Lague D., Hovius N. and Davy P., 2005. Discharge, discharge variability, and the bedrock channel profile. J. Geophys. Res., 110, F04006.

Lavé J. and Avouac J.P., 2001. Fluvial incision and tectonic uplift across the Himalayas of central Nepal. J. Geophy. Res., 106, B11: 25 561-25 593.

Lebrouc V., Schwartz S., Baillet L., Jongmans D. and Gamond J.F., 2013. Modeling permafrost extension in a rock slope since the Last Glacial Maximum: Application to the large Séchilienne landslide (French Alps). Geomorphology, 198, 198-200.

Lickorish H. W. and Ford M., 1998. Sequential restoration of the external Alpine Digne thrust system, SE France, constrained by kinematic data and synorogenic sediments. Geol. Soc.

Spec. Publ., 134, 189–211.

Mair D., Lechmann A., Yesilyurt S., Tikhomirov D., Delunel R., Vockenhuber C., Akçar N. and Schlunegger F., 2019. Fast long-term denudation rate of steep alpine headwalls inferred from cosmogenic $^{36}$Cl depth profiles. Scientific Reports, 9, 11023.

Mathey M., Sue C., Pagani C., Baize S., Walpersdorf A., Bodin T., Husson L., Hannouz E. and Potin B., 2020. Present-day geodynamics of the Western Alps: new insights from earthquake mechanisms. Solid Earth, 12, 1661-1681.

Mariotti A., Blard P.-H., Charreau J., Toucanne S., Jorry S.J., Molliex S., Bourlès D.L., Aumaître G. and Keddadouche K., 2021. Nonlinear forcing of climate on mountain denudation durings glaciations. Nat. Geosci., 14, 16-22.

Meigs A., Krugh W.C., Davis K. and Bank G., 2006. Ultra-rapid landscape response and sediment yield following glacial retreat, Icy Bay, soutehrn Alaska. Geomorphology, 78, 207-221.

Merchel S., Bremser W., Alfimov V., Arnold M., Aumaître G., Benedetti L., Bourlès D.L., Caffee M., Fifield L.K., Finkel R.C., Freeman S. P. H. T., Martschini M., Matsushi Y., Rood D.H., Sasa K., Steier P.,Takahashi T.,Tamari M., Tims S.G., Tosaki Y., Wilcken K.M. and Xu S., 2011. Ultra-trace analysis of $^{36}$Cl by accelerator mass spectrometry: an interlaboratory study , Anal. Bioanal. Chem., 400, 3125-3132.

Molnar P. and England P., 1990. Late Cenozoic uplift of mountain ranges and global change: chicken or egg? Nature, 346, 29-34.

Nocquet J.-M., Sue C., Walpersdorf A., Tran T., Lenôtre N., Vernant P., Cushing M., Jouanne F., Masson F., Baize S., Chéry J. and van der Beek P. A., 2016. Present-day uplift of the western Alps. Sci. Rep., 6, 28404.

Norton K.P., Abbühl L.M. and Schlunegger F., 2010. Glacial conditioning as an erosional driving force in the Central Alps. Geology, 38, 7, 655-658.

Nouibat A., Stehly L., Paul A., Schwartz S., Bodin T., Dumont T., Rolland Y., Brossier R. and CIFALPS Group, 2022. Lithospheric transdimensional ambient-noise tomography of W-Europe : implications for crustal-scale geometry of the W-Alps. Geophysical Journal International, 229, 862-879.

Ouimet W.B., Whipple K.X., Crosby B.T., Johnson J.P. and Schildgen T.F., 2008. Epigenetic gorges in fluvial landscapes. Earth Surf. Proc. Land., 33, 1993-2009.

Pan B., Burbank D.W., Wang Y., Wu G., Li J. et Guan Q., 2003. A 900 k.y. Record of strath terrace formation during glacial-interglacial transitions in northwest China. Geology, 31, 957-960.

Pratt B., Burbank D.W., Heimsath A. et Ojha T., 2002. Impulsive alluviation during early Holocene strengthened monsoons, central Nepal Himalaya. Geology, 30, 10, 911-914.

Penck W., 1924. Die morphologische analyse. Engelhorn's Nachfolger, Stuttgart, 283 p.

Petit C., Goren L., Rolland Y., Bourlès D., Braucher R., Saillard M. et Cassol D., 2017. Recent, climate-driven river incision rate fluctuations in the Mercantour crystalline massif, southern French Alps. Quaternary Sci. Rev., 165, 73-87.

Petit C., Rolland Y., Braucher R., Bourlès D., Guillou V. et Petitperrin V., 2019. River incision and migration deduced from 36Cl cosmic-ray exposure durations: The Clue de la Cerise gorge in southern French Alps. Geomorphology, 330, 81-88.

Petit C., Salles T., Godard V., Rolland Y. and Audin L. River incision, 10Be production and transport in a source-to-sink sediment system (Var catchment, SW Alps). EGUsphere [preprint].

Piña-Valdés J., Socquet A., Beauval C., Doin M.-P., D'Agostino N. and Shen Z.-K., 2022. 3D GNSS velocity field sheds light on the deformation mechanisms in Europe: Effects of the vertical crustal motion on the distribution of seismicity. Journal of Geophysical Research: Solid Earth, 127, e2021JB023451.

Protin M., Schimmelpfennig I., Mugnier J.-L., Ravanel L., Le Roy M., Deline P., Favier V., Buoncristiani J.-F. and ASTER Team, 2019. Climcatic reconstruction for the Younger Dryas/Early Holocene transtition and the Little Age based on paleo-extents of Argentière glacier (French Alps). Quaternary Sci. Rev., 221, 105863.

Rea B. R., Pellitero R., Spagnolo M., Hughes P., Ivy-Ochs S., Renssen H., Riboloni A., Bakke J., Lukas S. and Braithwaite R. J., 2020. Atmospheric circulation over Europe during the Younger Dryas. Sci. Adv., 6.

Renssen H., Seppä H., Heiri O., Roche D.M., Goosse H. and Fichefet T., 2009. The spatial and temporal complexity of the Holocene Thermal Maximum. Nature Geoscience 2, 411-414.

Renssen H., Seppä H., Crosta X., Goosse H. and Roche D.M., 2012. Global characterization of the Holocene Thermal Maximum. Quaternary Sci. Rev., , 48, 7-19.

Rolland Y., Petit C., Saillard M., Braucher R., Bourlès D., Darnault R., Cassol D. et ASTER Team, 2017. Inner gorges incision history: A proxy for deglaciation ? Insights from Cosmic Ray Exposure dating ($^{10}$Be and $^{36}$Cl) of river-polished surfaces (Tinée River, SW Alps, France). Earth Planet. Sci. Lett., 457, 271-281.

Rolland Y., Darnault R., Braucher R., Bourlès R., Petit C., Bouissou S. and ASTER Team, 2019. Deglaciation history at the Alpine-Mediterranean transition (Argentera-Mercantour, SW Alps) from $^{10}$Be dating of moraines and glacially polished bedrock. Earth Surf. Process. Landsforms, 45, 2, 393-410.

Royden L., and Perron J.T., 2013. Solutions of the stream power equation and application to the evolution of river longitudinal profiles, J. Geophys. Res. Earth Surf., 118, 497–518.

Sadier B., Delannoy J.-J., Benedetti L., Bourlès D.L., Jaillet S., Geneste J.-M., Lebatard A.-E. and Arnold M., 2012. Further constraints on the Chauvet cave artwork elaboration. PNAS, 109, 8002-8006.

Saillard M., Petit C., Rolland Y., Braucher R., Bourlès D. L., Zerathe S., Revel M. et Jourdon A., 2014. Late Quaternary incision rates in the Vésubie catchment area (Southern French Alps) from in situ-produced $^{36}$CI cosmogenic nuclide dating: Tectonic and climatic implications. J. Geophy. Res.. Earth Surface, 119, 1121-1135.

Sanchez G., Rolland Y., Corsini M., Braucher R., Bourlès D., Arnold M. and Aumaître G., 2010. Relationships between tectonics, slope instability and climate change: Cosmic Ray exposure dating of active faults, landslides and glacial surfaces in the SW Alps. Geomorphology, 107, 1-2, 1-13.

Sanchez G., Rolland Y., Jolivet M., Brichau S., Corsini M. and Carter A., 2011. Exhumation controlled by transcurrent tectonics: the Argentera–Mercantour massif (SW Alps). Terra Nova, 23, 2, 116-126.

Savi S., Norton K.P., Picotti V., Akçar N., Delunel R., Brardinoni F., Kubik P. and Schlunegger F., 2014. Quantifying sediment at the end of the last glaciation: Dynamic reconstruction of an alpine debris-flow fan. GSA Bulletin, 126, 5-6, 773-790.

Schaller M., Hovius N., Willett S.D., Ivy-Ochs S., Synal H.-A. and Chen M.-C., 2005. Fluvial bedrock incision in the active mountain belt of Taiwan from in situ-produced cosmogenic nuclides. Earth Surf. Proc. Land., 30, 955-971.

Schimmelpfennig I., Benedetti L., Finkel R., Pik R., Blard P.-H., Bourlès D.L., Burnard P. et Williams A., 2009. Source of in situ $^{36}$Cl in basaltics rocks. Implication for calibration of production rates. Quat. Geochronol., 4, 441-461.

Schwartz S., Gautheron C., Audin L., Dumont T., Nomade J., Barbarand J., Pinna-Jamme R. and van der Beek P., 2017. Foreland exhumation controlled by crustal thickening in the Western Alps. Geology, 45, 2, 139-142.

Seidl M.A. and Dietrich W.E., 1992. The problem of channel erosion into bedrock. Catena Supp., 23, 101-124.

Serpelloni E., Faccenna C., Spada G., Dong D. and Williams S. D. P., 2013. Vertical GPS ground motion rates in the Euro-Mediterranean region: New evidence of velocity gradients at different spatial scales along the Nubia-Eurasia plate boundary. J. Geophys. Res.: Solid Earth, 118, 6003-6024.

Sklar L. S. and Dietrich W. E., 2001. Sediment and rock strength controls on river incision into bedrock. Geology, 29, 12, 1087-1090.

Sternai P., Sue C., Husson L., Serpelloni E., Becker T.W., Willet S.D., Faccenna C., Giulio A.D., Spada G., Jolivet L., Valla P., Petit C., Nocquet J. M., Walpersdorf A. and Castelletort S., 2019. Present-day uplift of the European Alps: Evaluating mechanisms and models of their relative contributions. Earth-Sci. Rev., 190, 589-604.

Sternai P., Herman F., Valla P. G. and Champagnac J.-D., 2013. Spatial and temporal variations of glacial erosion in the Rhône valley (Swiss Alps): Insights from numerical modeling. Earth Planet. Sci. Lett., 368, 119-131.

Stock J.D., Montgomery D.R., Collins B.D., Dietrich W.E. and Sklar L., 2005. Field measurements of incision rates following bedrock exposure: implications for process controls on the long profiles of valleys cut by rivers and debris flows. GSA Bulletin, 117, 11-12, 174-194.

Stock J.D. and Montgomery D.R., 1999. Geologic constraints on debrock river incision using the stream power law. J. Geophys. Res., 104, B3, 4983-4993.

Stone J.O., 2000. Air pressure and cosmogenic isotope production. J. Geophys. Res.: Solid Earth, 105, 23,753-23,759.

Sue C. and Tricart P., 1999. Late alpine brittle extension above the Frontal Pennine Thrust near Briançon, western Alps. Eclogae Geol. Helv., 92, 2, 171-181.

Sue C., Delacou B., Champagnac J.-D., Allanic C. and Burkhard., 2007. Aseismic deformation in the Alps: GPS vs. seismic strain quantification. Terra Nova, 1, 182-188.

Tucker G.E. and Whipple K.X., 2002. Topographic outcomes predicted by stream erosion models: Sensitivity analysis and intermodel comparison. J. Geophy. Res., 107, B9, ETG 1-1-ETG 1-16.

Vacchi M., Marriner N., Morhange C., Spada G., Fontana A. and Alessio R., 2016. Multiproxy assessment of Holocene relative sea-level changes in the western Mediterranean: sea-level variability and improvements in the definition of the isostatic signal. Earth-Sci. Rev, 155, 172-197.

Valla P.G., van der Beek P.A. et Carcaillet J., 2010. Dating bedrock gorge incision in the French Western Alps (Ecrin-Pelvoux massif) using cosmogenic 10Be. Terra Nova, 22, 18-25.

Valla P.G., Shuster D.L. et Van der Beek P.A., 2011. Significant increase in relief of the European Alps during mid-Pleistocene glaciations. Nat. Geoscience, 4, 688–692.

Van den Berg F., Schlunegger F., Akçar N. and Kubik P., 2012. 10Be-derived assessment of accelerated erosion in a glacially conditioned inner gorge, Entlebuch, Central Alps of Switzerland. Earth Surf. Process. Landforms, 37, 11, 1175-1188.

van der Beek P. and Bourbon P., 2008. A quantification of the glacial imprint on relief development in the French western Alps. Geomorphology, 97, 52-72.

van der Woerd J., Tapponnier P., Ryerson F.J., Meriaux A.-S., Meyer B., Gaudemer Y., Finkel R.C., Caffee M.W., Zhao G. et Xu Z., 2002. Uniform postglacial slip-rate along the central 600 km of the Kunlun Fault (Tibet), from $^{26}$Al, $^{10}$Be, and $^{14}$C dating of riser offsets, and climatic origin of the regional morphology. Geophys. J. Int., 148, 356-388.

Walpersdorf A., Pinget L., Vernant O., Sue C., Deprez A. and RENAG team, 2018. Does long-term GPS in the Western Alps finally confirm earthquake mechanisms? Tectonics, 37, 3721-3737.

Wanner H., Beer J., Bütikofer J., Crowley T.J., Cubash U., Flückiger J., Goosse H., Grosjean

M., Joos F., Kaplan J.O., Küttel M., Müller S.A., Prentice I.C., Solomina O., Stocker T.F., Tarasov P., Wagner M. and Widmann M., 2008. Mid- to Late Holocene climate change: an overview. Quaternary Sci. Rev., 27, 1791-1828.

Wanner H., Solomina O., Grosjean M., Ritz S.P. and Markéta J., 2011. Structure and origin of Holocene cold events. Quaternary Sci. Rev., 30, 3109-3123.

Wanner H., Mercolli L., Grosjean M. and Ritz S.P., 2015. Holocene climate variability and change: a data-based review. J. Geol. Soc. London, 172, 254-263.

Whipple K.X. et Tucker G.E., 1999. Dynamics of the stream-power river incision model: Implications for height limits of mountain ranges, landscape response timescales, and research needs. J. Geophy. Res., 104, 17,661–17,674.

Whipple K.X., Hancock G.S. and Anderson R.S., 2000. River incision into bedrock: Mechanics and relaive efficacy of plucking, abrasion, and cavitation. GSA Bulletin, 112, 3, 490-503.

Whipple K.X., 2001. Fluvial landscape response time: how plausible is steady-state denudation? Am. J. Sci., 301, 313-325.

Whipple K.X. et Tucker G.E., 2002. Implications of sediment- flux- dependent river incision models for landscape evolution. J. Geophy. Res., 107, B2, ETG 3-1-ETG 3-20.

Willet S.D., 1999. Orogeny and orography: the effects of erosion on the structure of mountain belts. J. Geophy. Res., 104, B12, 28 957-28 981.

Willet S.D., Slingerland R. et Hovius N., 2002. Uplift, shortening, and steady-state topography in active mountain belts. Am. J. Sci., 301, 455-485.

Wobus C., Whipple K.X., Kirby E., Snyder N., Johnson J., Spyropolou K., Crosby B. et Sheehan D., 2006. Tectonics from topography: procedures, promise, and pitfalls. In: Willett S.D., Hovius N., Brandon M.T., Fisher D.M., (Eds.), Tectonics, Climate, and Landscape Evolution. Geol. Soc. Am. Bull. Special Paper, 398, 55-74.

Zerathe S., Lebourg T., Braucher R. and Bourlès D., 2014. Mid-Holocene cluster of larger-scale landslides revealed in the Southwestern Alps by $^{36}Cl$ dating. Insight on an Alpine-Scale landslide activity. Quaternary Sci. Rev., 90, 106-127.

**Declaration of interests**

☒The authors declare that they have no known competing financial interests or personal relationships that could have appeared to influence the work reported in this paper.

☐The authors declare the following financial interests/personal relationships which may be considered as potential competing interests:

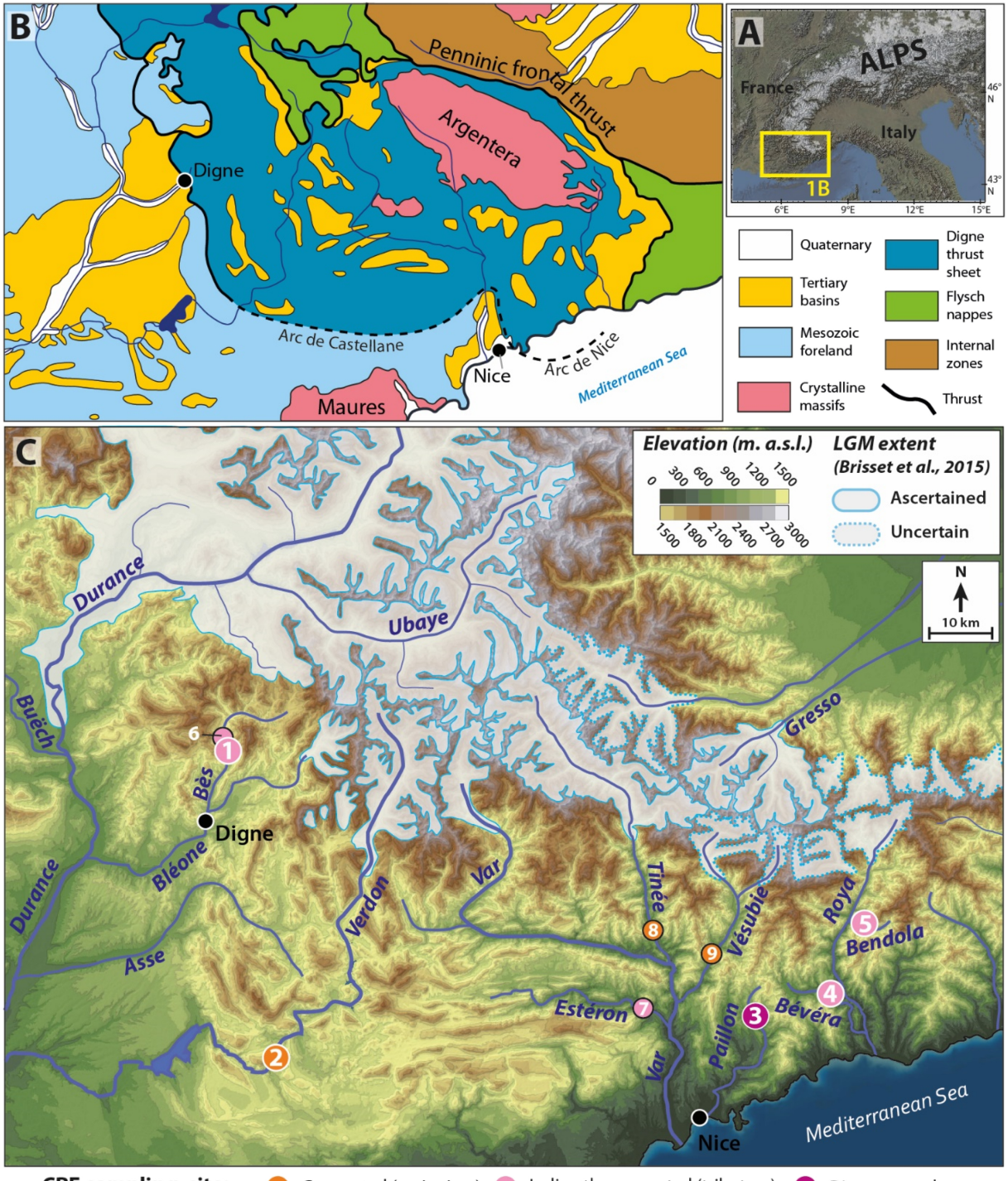
B
Penninic frontal thrust
Argentera
Digne
Arc de Castellane
Arc de Nice
Nice
Maures
Mediterranean Sea
A
ALPS
France
Italy
1B
46° N
43° N
6°E
9°E
12°E
15°E
Quaternary
Tertiary basins
Mesozoic foreland
Crystalline massifs
Digne thrust sheet
Flysch nappes
Internal zones
Thrust
C
Elevation (m. a.s.l.)
0 300 600 900 1200 1500
1500 1800 2100 2400 2700 3000
LGM extent (Brisset et al., 2015)
Ascertained
Uncertain
N
10 km
Durance
Ubaye
Buëch
Bès
Digne
Bléone
Asse
Verdon
Var
Tinée
Vésubie
Gresso
Roya
Bendola
Bévéra
Paillon
Estéron
Mediterranean Sea
Nice
1
2
3
4
5
6
7
8
9
CRE sampling site:
Connected (main river)
Indirectly-connected (tributary)
Disconnected

Figure 1

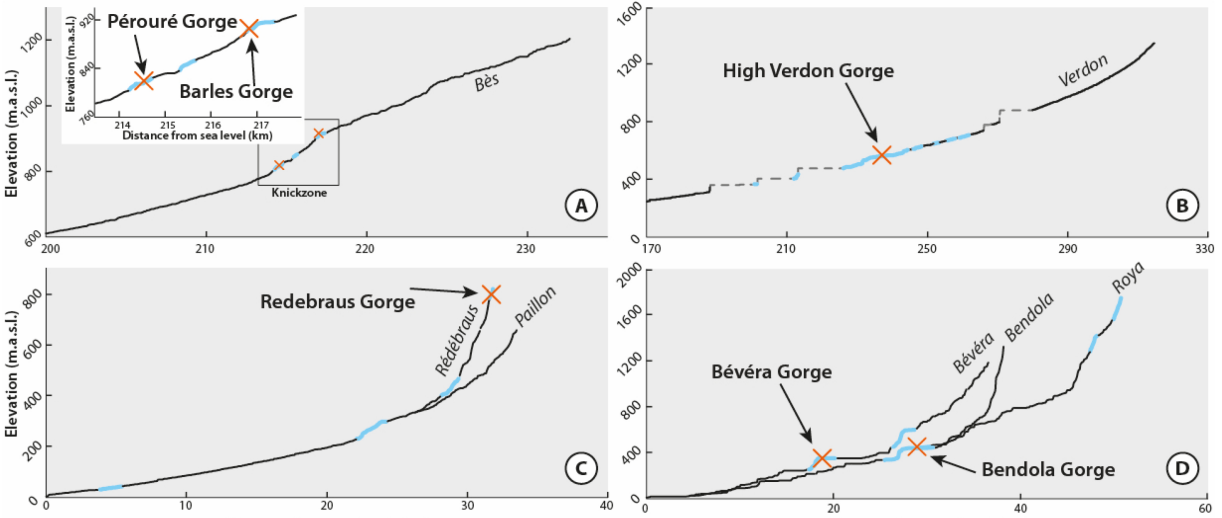
Pérouré Gorge
Barles Gorge
Elevation (m.a.s.l.)
Distance from sea level (km)
Bès
Knickzone
A
High Verdon Gorge
Verdon
B
Redebraus Gorge
Rédébraus
Paillon
C
Bévéra Gorge
Bévéra
Bendola
Roya
Bendola Gorge
D

Figure 2

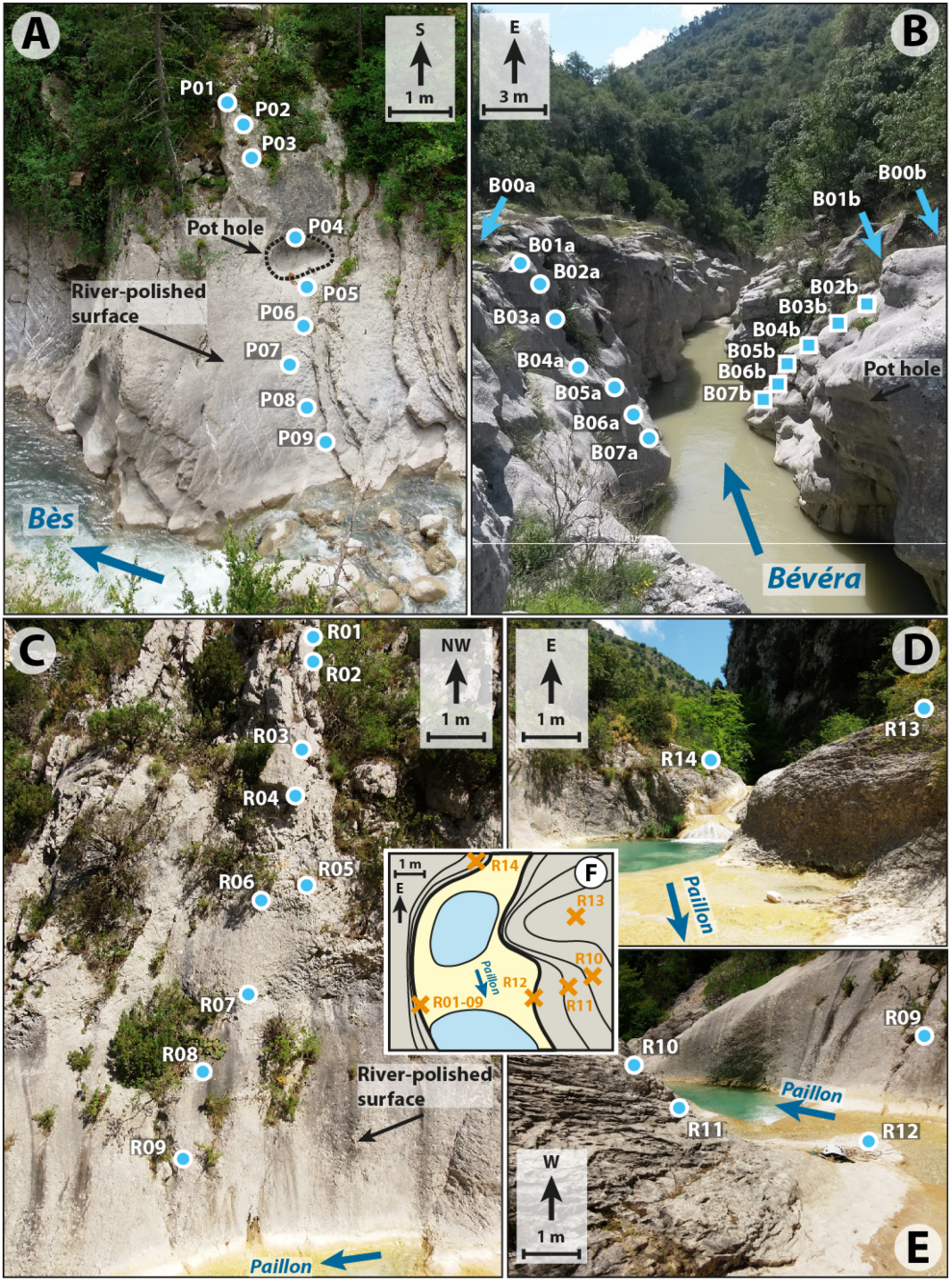
A
S
1 m
P01
P02
P03
Pot hole
P04
River-polished surface
P05
P06
P07
P08
P09
Bès
B
E
3 m
B00a
B00b
B01b
B01a
B02a
B02b
B03b
B03a
B04b
B05b
B06b
B07b
Pot hole
B04a
B05a
B06a
B07a
Bévéra
C
NW
1 m
R01
R02
R03
R04
R06
R05
R07
R08
R09
River-polished surface
Paillon
D
E
1 m
R13
R14
Paillon
F
1 m
E
R14
R13
R10
Paillon
R12
R11
R01-09
E
R09
R10
Paillon
R11
R12
W
1 m

Figure 3

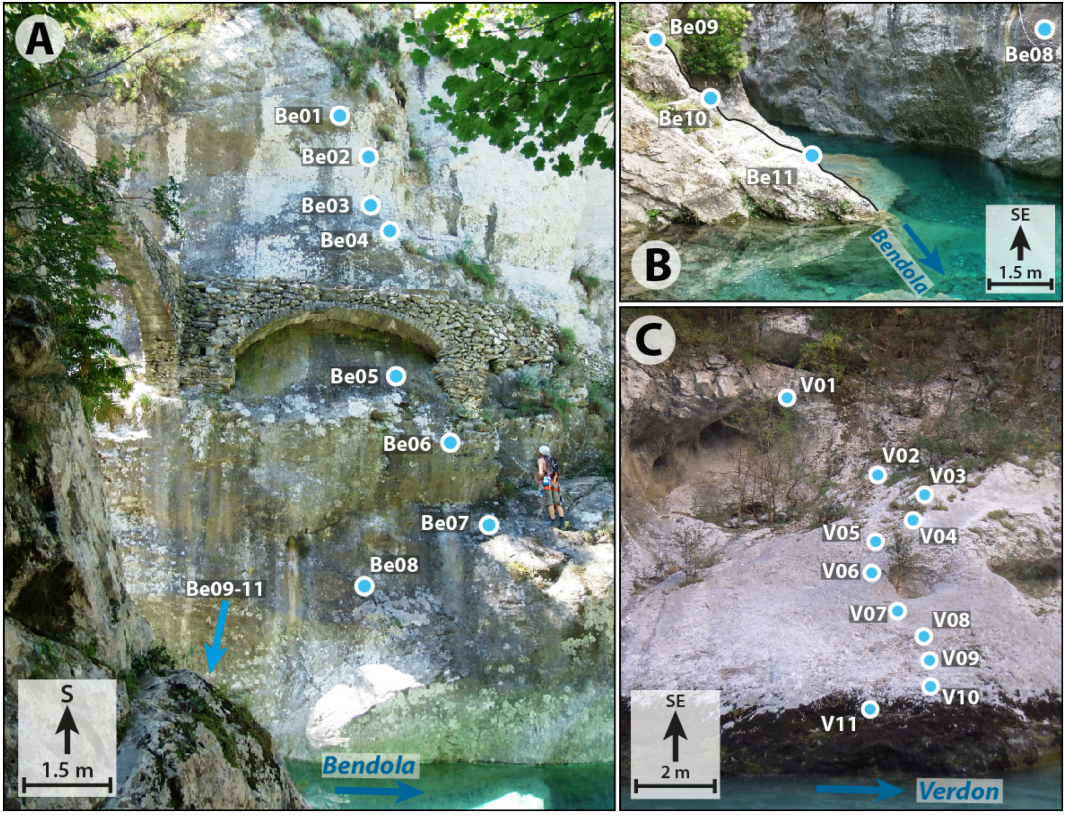
A
Be01
Be02
Be03
Be04
Be05
Be06
Be07
Be08
Be09-11
S
1.5 m
Bendola
B
Be09
Be08
Be10
Be11
SE
1.5 m
Bendola
C
V01
V02
V03
V04
V05
V06
V07
V08
V09
V10
V11
SE
2 m
Verdon

Figure 4

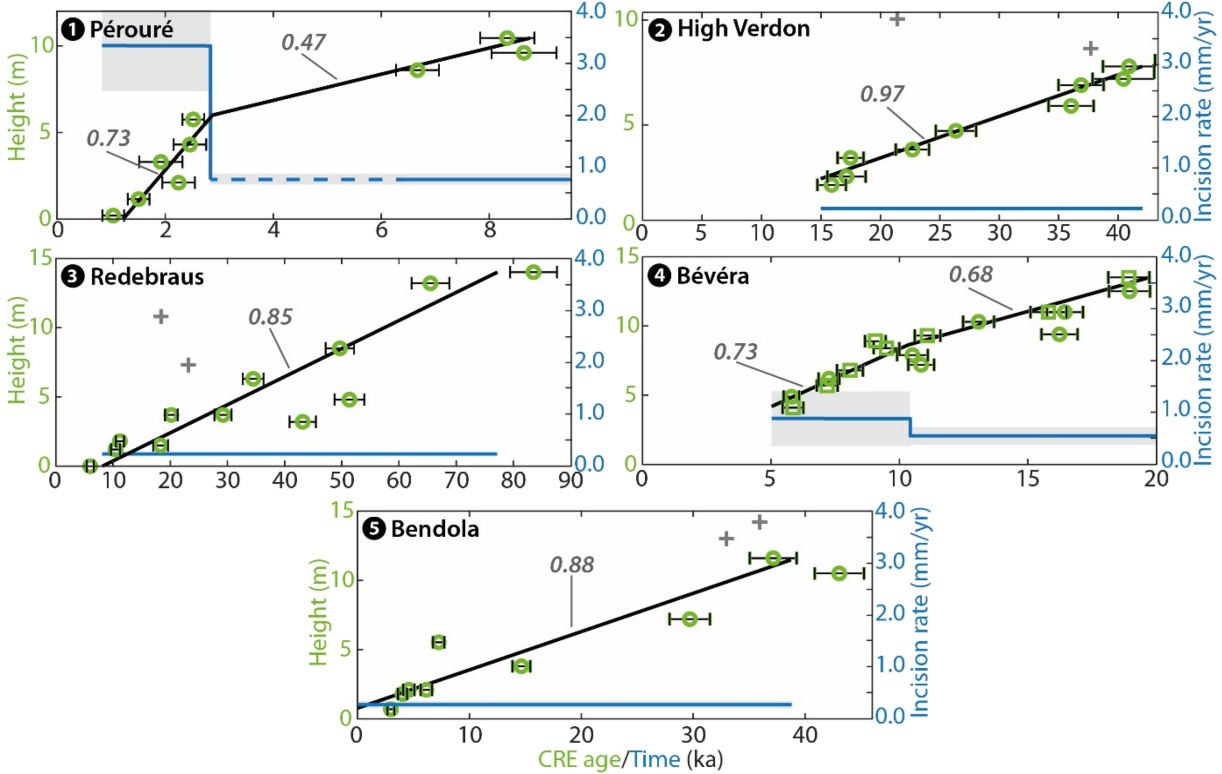
1 Pérouré
0.47
0.73
2 High Verdon
0.97
3 Redebraus
0.85
4 Bévéra
0.68
0.73
5 Bendola
0.88
Height (m)
Incision rate (mm/yr)
CRE age/Time (ka)

Figure 5

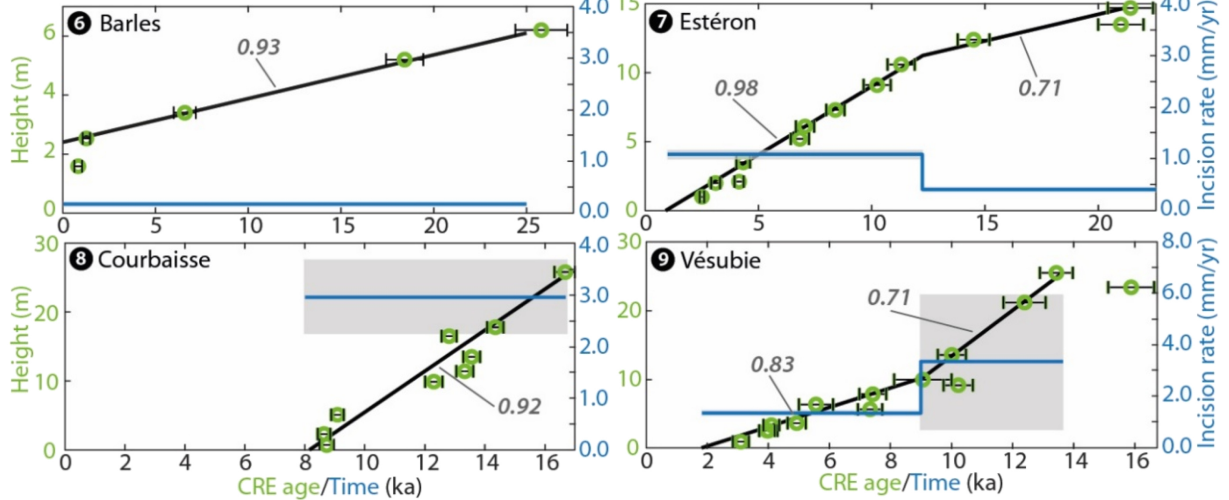
6 Barles
0.93
Height (m)
7 Estéron
0.98
0.71
Incision rate (mm/yr)
8 Courbaisse
0.92
9 Vésubie
0.71
0.83
CRE age/Time (ka)

Figure 6

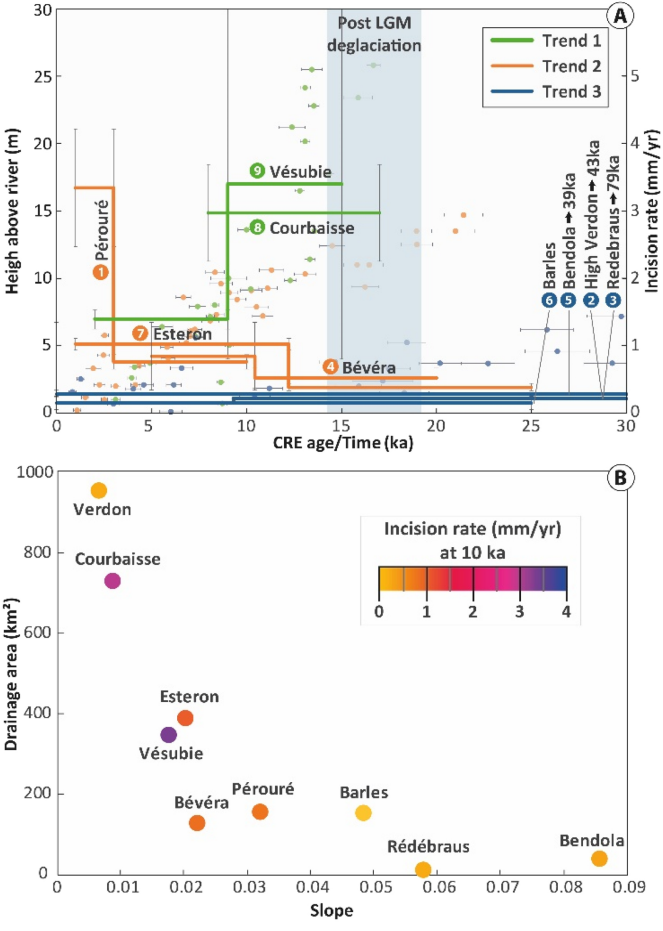
A
Post LGM deglaciation
Trend 1
Trend 2
Trend 3
Heigh above river (m)
Incision rate (mm/yr)
CRE age/Time (ka)
1 Pérouré
9 Vésubie
8 Courbaisse
7 Esteron
4 Bévéra
6 Barles
5 Bendola → 39ka
2 High Verdon → 43ka
3 Redebraus → 79ka
B
Incision rate (mm/yr) at 10 ka
Drainage area (km²)
Slope
Verdon
Courbaisse
Esteron
Vésubie
Bévéra
Pérouré
Barles
Rédébraus
Bendola

Figure 7

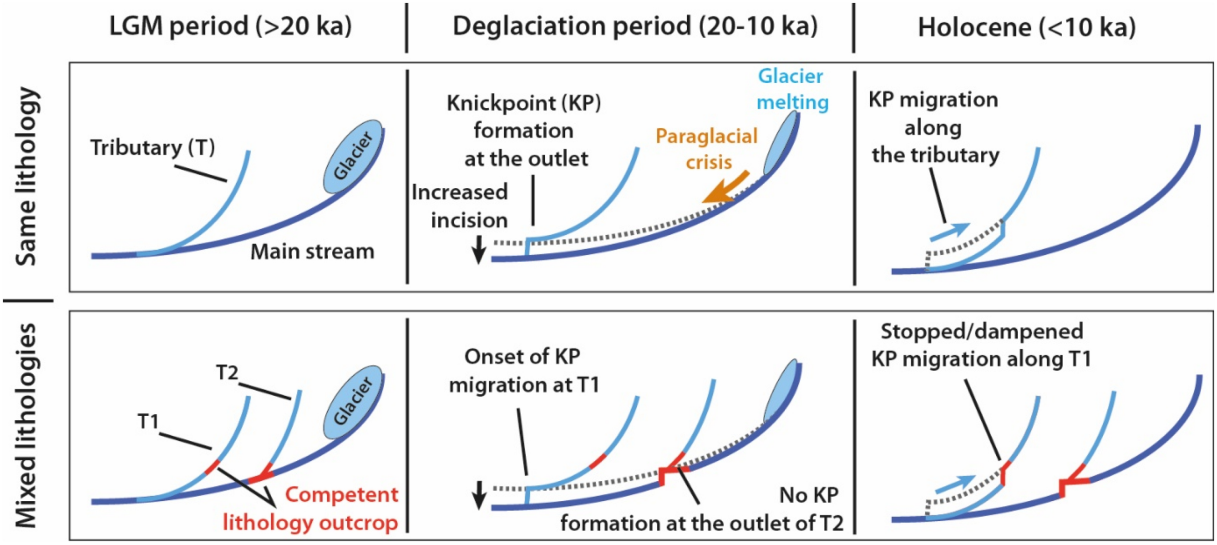
LGM period (>20 ka)
Deglaciation period (20-10 ka)
Holocene (<10 ka)
Same lithology
Mixed lithologies
Tributary (T)
Glacier
Main stream
Knickpoint (KP) formation at the outlet
Increased incision
Paraglacial crisis
Glacier melting
KP migration along the tributary
T2
T1
Glacier
Competent lithology outcrop
Onset of KP migration at T1
No KP formation at the outlet of T2
Stopped/dampened KP migration along T1

Figure 8